Cell

WNT/TCF Signaling through LEF1 and HOXB9 Mediates Lung Adenocarcinoma Metastasis

Don X. Nguyen,[1] Anne C. Chiang,[2] Xiang H.-F. Zhang,[1] Juliet Y. Kim,[1] Mark G. Kris,[2,5] Marc Ladanyi,[3,4] William L. Gerald,[3,4] and Joan Massagué[1,6,*]
[1]Cancer Biology and Genetics Program
[2]Department of Medicine
[3]Department of Pathology
[4]Human Oncology and Pathogenesis Program
[5]Weill Medical College of Cornell University
[6]Howard Hughes Medical Institute
Memorial Sloan-Kettering Cancer Center, New York, NY, USA
*Correspondence: j-massague@ski.mskcc.org
DOI 10.1016/j.cell.2009.04.030

SUMMARY

Metastasis from lung adenocarcinoma can occur swiftly to multiple organs within months of diagnosis. The mechanisms that confer this rapid metastatic capacity to lung tumors are unknown. Activation of the canonical WNT/TCF pathway is identified here as a determinant of metastasis to brain and bone during lung adenocarcinoma progression. Gene expression signatures denoting WNT/TCF activation are associated with relapse to multiple organs in primary lung adenocarcinoma. Metastatic subpopulations isolated from independent lymph node-derived lung adenocarcinoma cell lines harbor a hyperactive WNT/TCF pathway. Reduction of TCF activity in these cells attenuates their ability to form brain and bone metastases in mice, independently of effects on tumor growth in the lungs. The WNT/TCF target genes *HOXB9* and *LEF1* are identified as mediators of chemotactic invasion and colony outgrowth. Thus, a distinct WNT/TCF signaling program through LEF1 and HOXB9 enhances the competence of lung adenocarcinoma cells to colonize the bones and the brain.

For a video summary of this article, see the PaperFlick file available with the online Supplemental Data.

INTRODUCTION

Metastasis is an ominous feature of malignant solid tumors, and its natural course varies extensively depending on the type of disease. The tissue and cell of origin of the tumor markedly influence the sites and severity of distant metastasis. Depending on the cancer subtype, metastasis may emerge quickly in multiple organs or in particular organs after a protracted latency period. Breast tumors, for example, undergo dissemination from an early stage (Husemann et al., 2008; Klein et al., 1999), but metastasis to bones, lungs, brain, or liver may not manifest until years or decades after the diagnosis and removal of the primary tumor (Karrison et al., 1999; Schmidt-Kittler et al., 2003). This course suggests that disseminated breast cells normally require further malignant evolution to overtly colonize distant organs. This process gives rise to organ-specific metastatic cell populations, which has prompted the identification of organ-specific metastasis genes and functions (Nguyen et al., 2009).

Metastasis in other types of cancer follows a different course, with rapid spread to multiple organs. A case in point is lung adenocarcinoma, the most common subtype of lung cancer with a high mortality rate (Hoffman et al., 2000). Even if diagnosed at an early stage and surgically removed, lung adenocarcinomas can relapse within months, spreading to the lymph nodes, contralateral lung, adrenal glands, the bones, and the brain (Feld et al., 1984; Hess et al., 2006; Martini et al., 1995). Brain metastasis has particularly morbid physical and cognitive consequences (Gaspar, 2004; Gavrilovic and Posner, 2005; Thomas et al., 2000). Lung adenocarcinoma is a principal source of brain metastasis, due in part to the arterial circulation flowing directly from the lungs to the brain, which pulmonary cancer cells can more easily access (Gaspar, 2004; Gavrilovic and Posner, 2005; Thomas et al., 2000).

The genes and mechanisms that mediate lung adenocarcinoma metastasis are largely unknown. However, the natural course of this disease suggests the acquisition of mechanisms in lung adenocarcinoma cells that allow the aggressive infiltration and colonization of multiple organs soon after cancer cell dispersion from a primary tumor. This hypothesis led us to consider the involvement of developmental pathways as providers of these functions. By combining genome-wide transcriptional analysis and experimental modeling, we identified the activation of the WNT/TCF pathway as a determinant of lung adenocarcinoma metastatic competence to multiple organ sites.

The WNT signaling pathway plays major roles in stem cell biology, organogenesis, tissue homeostasis, and cancer (Clevers,

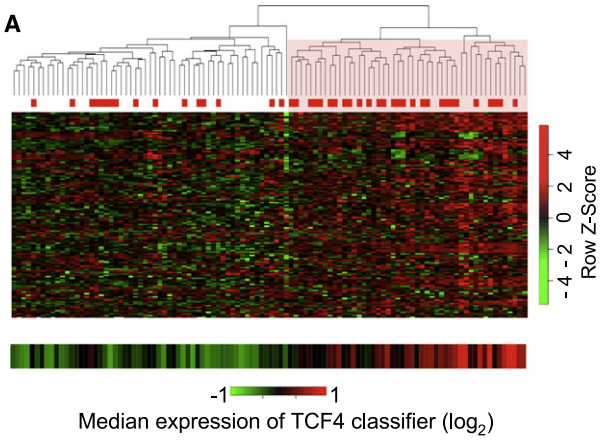

C

Pathway signature	Lung adenocarc. recurrence	Breast cancer recurrence
TGFβ	0.54	0.02
KRAS	0.28	0.35
TCF4	0.006	0.11
SRC	0.193	0.62
E2F3	0.402	(0.04)
MYC	0.03	0.36

Figure 1. A Subset of TCF4 Target Genes Associated with Lung Adenocarcinoma Metastasis

(A) Hierarchical clustering of 107 clinically annotated human lung adenocarcinomas (MSKCC set 1) using a list of 73 TCF4 regulated genes available on the U133A Affymetrix chip, segregates a set of tumors (red block) with a high proportion of relapses (red bars). R value = 0.73. The bottom row represents the median expression value of TCF4 target genes.

(B) Kaplan-Meier curves for metastasis-free survival to all sites according to TCF4 signature.

(C) Metastasis-free prediction of other pathway classifiers in MSKCC set 1 and a cohort of 368 primary breast tumors. The p value in parentheses denotes inverse correlation. p values were calculated by log rank test.

2006; Klaus and Birchmeier, 2008; Logan and Nusse, 2004; Moon et al., 2004). Binding of secreted Wnt ligands to Frizzled and LRP5/6 transmembrane receptors prevents the phosphorylation-dependent polyubiquitination and degradation of the signaling pool of β-catenin in the cytoplasm. This degradation is initiated by a protein complex including APC (the *adenomatous polyposis coli* gene product), Axin, and glycogen synthase kinase-3β (GSK-3β) (Clevers, 2006; Logan and Nusse, 2004). Spared from degradation, β-catenin accumulates in the nucleus and binds to transcription factors of the LEF/TCF (lymphoid enhancer-binding factor and T cell factor) family to regulate gene expression (Arce et al., 2006).

Mutations that constitutively activate the WNT pathway are frequently involved in colorectal cancer initiation (Clevers, 2006; Moon et al., 2004; Morin et al., 1997; Polakis, 2007). However, such mutations are infrequent in lung adenocarcinomas (Ding et al., 2008; Mazieres et al., 2005). Prominent tumor-initiating events in lung adenocarcinoma include KRAS and EGFR mutations (Rodenhuis et al., 1988; Sharma et al., 2007). Surprisingly, we found that gene-expression signatures denoting WNT/TCF pathway activity in lung adenocarcinomas are associated with a high rate of relapse to distant sites. In vivo selection of metastatic cells from independent human lung adenocarcinoma lines yields derivatives that harbor a hyperactive WNT/TCF pathway, in association with an enhanced ability to infiltrate and colonize the brain and bones. Using these cells as a model, we provide functional evidence for the involvement of two WNT target genes, the transcription factors *HOXB9* and *LEF1*, as mediators of chemotactic invasion and colony outgrowth.

RESULTS

A TCF Transcriptional Signature Is Associated with Lung Adenocarcinoma Relapse

Because of the propensity of lung adenocarcinomas to rapidly metastasize to multiple organs, and the lack of mutations associated with this transition thus far, we undertook the approach of analyzing a clinical cohort of lung adenocarcinomas using gene-expression signatures that denote activation of specific pathways. We utilized gene sets that were responsive to a K-Ras mutation in a mouse model (Sweet-Cordero et al., 2005), to a dominant-negative TCF4 (dnTCF4) in colon cancer cells (van de Wetering et al., 2002), to treatment of epithelial cells with TGF-β (Padua et al., 2008), or to overexpression of c-Myc, SRC, or E2F3 in human mammary epithelial cells (Bild et al., 2006). We queried gene-expression data on 107 annotated primary lung adenocarcinomas including 65 stage I tumors from patients who had relapsed and who remained disease free (MSKCC set 1, Table S1 available online). In an unsupervised analysis, the TCF4 gene signature identified a distinct subgroup (Figure 1A) with an elevated rate of recurrence to multiple organs (Figure 1B, p = 0.006). The K-Ras, SRC, and E2F3 signatures were not predictive of increased overall metastasis (Figure 1C). The TGF-β signature, which is associated with lung relapse in estrogen receptor-negative breast tumors (Padua et al., 2008) was not specifically associated with lung adenocarcinoma metastasis, whereas the MYC signature was modestly predictive (Figure 1C, p = 0.03). A β-catenin gene set (Bild et al., 2006) was not associated with relapse (data not shown). This set, however, largely consists of downregulated genes in the absence of Wnt signal, potentially reflecting context-specific β-catenin functions that are independent of TCF transcription (Gottardi and Gumbiner, 2004). After statistical correction for multiple comparisons, the TCF4 gene set was the only significant predictor of relapse (Bonferroni correction, p = 0.042). Because TCF4 is a member of the LEF/TCF family of WNT pathway transcriptional effectors (Arce et al., 2006), we postulated that canonical WNT transcriptional activity may distinguish a subset of lung adenocarcinomas with high competence for metastasis.

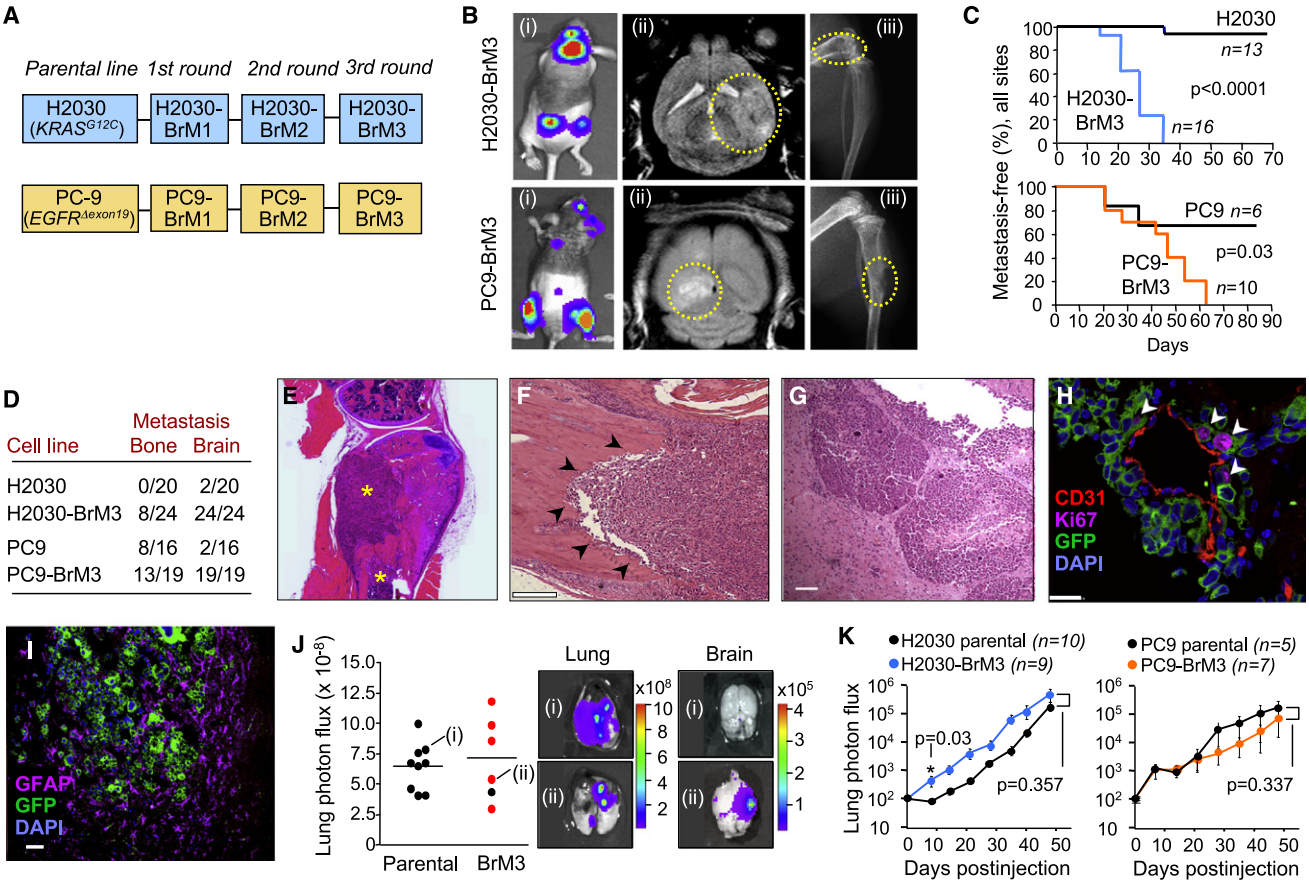

Figure 2. Experimental Model of Lung Adenocarcinoma Metastasis

(A) In vivo selection scheme for the isolation of metastatic populations (BrM3) from the NCI-H2030 and PC9 lung adenocarcinoma lines.

(B) Shown are representative bioluminescent images (i) of brain, limb and spine metastasis. Brain and bone lesions were confirmed via MRI (ii) and X-ray, respectively (iii).

(C) Kaplan-Meier curves of metastasis incidence (brain and/or bone) in mice inoculated with 10^4 cells. Parental H2030 cells versus H2030-BrM3 derivatives are (top) and PC9 parental versus PC9-BrM3 cells (bottom) are shown. p values were calculated by log rank test.

(D) Frequency and distribution of metastasis after inoculation of 5×10^4 cells.

(E) Hematoxylin and eosin (H&E) stain of hind limb. * indicates bone lesions.

(F) H&E stain of osteolytic metastasis (arrows). The scale bar represents 200 μm.

(G) H&E staining of PC9-BrM3 brain metastasis. The scale bar represents 100 μm.

(H) Confocal imaging of H2030-BrM3 cells in the brain (GFP, green), human Ki67 (magenta), CD31+ vasculature (red), and DAPI (blue). Arrows indicate Ki67-positive tumor cells. The scale bar represents 23 μm.

(I) PC9-BrM3 tumor (GFP, green), surrounded by reactive astrocytes expressing glial fibrillary acidic protein (GFAP, magenta). The scale bar represents 50 μm.

(J) H2030 parental and H2030-BrM3 cells were implanted with Matrigel in the lung via intrathoracic inoculation. Tumors were grown for 6–8 weeks before organs were extracted and imaged. Left: scatter plot of lung photon flux for parental and BrM3-injected mice with a similar range of lung tumor burden. The absence (black dot) or presence (red dot) of brain metastasis is noted for each animal. Right: representative images of lungs inoculated with parental (i) or BrM3 (ii) cells and corresponding brains.

(K) Lung/pleural tumor growth rates were measured after intrathoracic implantation. Data are presented as the normalized mean lung photon flux. Error bars represent the SEM. p values are based on a two-sided Student's t test. n, number of animals per cohort.

An Experimental Model of Lung Adenocarcinoma Metastasis

To develop an experimental model for the analysis of lung adenocarcinoma metastasis, we isolated metastatic subpopulations from two human lung cancer cell lines. The H2030 cell line was established from a lymph node of a stage III lung adenocarcinoma patient and harbors a *KRAS*^{G12C} mutation (Phelps et al., 1996). The PC9 line was established from a lymph node of a lung adenocarcinoma patient with an *EGFR*$^{\Delta exon19}$ mutation (Koizumi et al., 2005; Sasaki et al., 1991). As these two cell lines were derived from lymph nodes, they provided appropriate systems for the isolation of malignant cells that might harbor multiorgan metastatic competence before adaptation to grow in distant organs.

When placed in the arterial circulation of immunodeficient mice by intracardiac inoculation, both cell lines colonized the bones and brain. We extracted tumor cells from the brain and expanded them in culture for two more rounds of in vivo selection (Figure 2A). The resulting BrM3 cell populations consistently

demonstrated enriched metastatic activity, as detected by bioluminescence imaging (BLI) and magnetic resonance of the brain or X-ray imaging of the bones (Figure 2B). H2030-BrM3 and PC9-BrM3 cells formed brain metastasis in 100% of animals compared to a 10%–13% efficiency of the parental lines (Figures 2C and 2D). Although isolated from the brain, the H2030-BrM3 and, to a lesser extent, PC9-BrM3 cells showed an increased ability to colonize the vertebral and limb bones over their starting metastatic potential (Figure 2D). Thus, the ability to metastasize to bone and brain are linked in the BrM3 derivatives.

In the bones, PC9-BrM3 and H2030-BrM3 formed osteolytic lesions (Figures 2E and 2F). PC9-BrM3 and H2030-BrM3 cells avidly colonized the cerebrum and cerebellum, forming nodules, as well as smaller invasive lesions with occasional spread into the meninges (Figure 2G and Figure S1A). Invasive metastases in the brain were not angiogenic, but displayed perivascular localization and proliferation (Figure 2H), with gliosis (Figure 2I) and astrocyte proliferation at the invasive edge of metastasis (Figure S1B). Importantly, H2030-BrM3 cells implanted orthotopically in the lung could disseminate to the brain independently of lung and pleural tumor burden (Figure 2J).

BrM3 cells did not proliferate faster than their parental populations in monolayer culture, nor were they more resistant to growth factor depletion (Figures S2A and S2B). When implanted with extracellular matrix Matrigel directly into the lungs, H2030-BrM3 cells had an initial growth advantage (Figure 2K, left), whereas PC9-BrM3 cells did not have altered tumorigenic rates compared to their parental counterparts (Figure 2K, right). Similar results were obtained from subcutaneously implanted tumors (data not shown). The advantage of H2030-BrM3 cells is consistent with their enhanced colony-forming ability in Matrigel (see below). However, the subsequent expansion rate of H2030-BrM3 tumors in the lung over 7 weeks was not significantly different from those of the parental line (Figure 2K, left). In sum, these two lung adenocarcinoma models recapitulate salient features of metastasis from lung adenocarcinoma, including the capacity to rapidly disseminate and colonize bone and brain.

Deregulated WNT/TCF Activity in Highly Metastatic Lung Adenocarcinoma Cells

We analyzed the transcriptome of the parental and BrM3 derivatives under basal cell culture conditions. The PC9-BrM3 transcriptome was significantly enriched for the TCF4 classifier, and the H2030-BrM3 cells showed a detectable albeit not statistically significant enrichment (Figure 3A). To evaluate the overall activity of WNT/TCF pathway in these cell lines, we performed transcriptional reporter assays using the TOP/FOP reporter system (Korinek et al., 1997). The BrM3 cells in both systems showed higher basal TCF transcriptional activity (2-fold and 2.8-fold, respectively) than the corresponding parental lines (Figure 3B). Furthermore, addition of the ligand Wnt3A caused a strong increase in TCF activity in the BrM3 subpopulations, which significantly surpassed the Wnt3a-induced increase in the parental lines (Figure 3B). These results revealed the presence of a deregulated TCF pathway in both metastatic cell populations.

β-catenin is distributed as an abundant membrane associated pool and a free labile pool available for WNT/TCF signaling. The stabilization and nuclear localization of this free pool are necessary for β-catenin as a coactivator of TCF-dependent transcription (Clevers, 2006; Klaus and Birchmeier, 2008; Logan and Nusse, 2004; Moon et al., 2004). Immunoblotting analysis revealed nuclear accumulation of β-catenin after Wnt3a treatment in all adenocarcinoma lines (Figure 3C). Notably, both the cytosolic and nuclear/signaling levels of β-catenin were higher in BrM3 cells than in parental H2030 cells (Figure 3C). Phosphorylation of β-catenin at Ser33/37 and Thr41 marks the signaling pool for proteosomal degradation (Clevers, 2006). Upon Wnt3A stimulation, β-catenin was more rapidly dephosphorylated at Ser33/37 and Thr41 in H2030-BrM3 cells, indicating a greater rate of stabilization (Figure 3D). In the PC9 derivatives, β-catenin was abundant in both parental and BrM3 cells, suggesting the preexistence of a hyperactive WNT pathway (Figure 3C). Dephosphoryation of Ser33/37 and Thr41 in response to Wnt3a was similar in the parental and BrM3 PC9 lines, suggesting that enhanced TCF activity in PC9-BrM3 cells may depend on additional alterations (Figure 3D).

Somatic mutations in *APC* or the β-catenin gene (*CTNNB1*) can increase β-catenin stability and activity in colorectal cancer (Clevers, 2006; Moon et al., 2004; Morin et al., 1997; Polakis, 2007). Mutations in these genes have been detected at low frequency in lung adenocarcinomas (Ding et al., 2008). In BrM3 and parental sets, we sequenced *APC*, *CTNNB1*, and 13 additional genes (*APC2*, *AXIN1*, *AXIN2*, *GSK3B*, *STK11*, *LEF1*, *TCF7/TCF1*, *TCF7L1/TCF3*, *TCF7L2/TCF4*, *FRZB*, *SFRP1*, *SFRP2*, and *SFRP4*) that encode proximal components of the WNT pathway. No mutations were found to be specifically associated with BrM3 populations, except for a silent mutation in *SFRP4* (G to A, chromosome 7: 37918251) in H2030-BrM3 cells. qRT-PCR and GeneChip array analysis of 84 WNT pathway-related genes (including those sequenced) revealed a common upregulation of *LEF1* in highly metastatic cells (Figures 3E and 3F), with less consistent alteration in the expression of the other genes (data not shown). These results suggest that hyperactivation of WNT/TCF in these metastatic cells is not due to mutations in core components of the WNT pathway but to other alterations that commonly converge on WNT transcriptional effectors.

A Lung Adenocarcinoma WNT Gene Response Associated with Metastasis

Because the TCF4 signature was obtained from a colon cancer cell line (van de Wetering et al., 2002) we asked whether the metastatic potential of lung adenocarcinomas also correlates with WNT gene-expression responses derived specifically from lung adenocarcinoma cells. We generated transcriptomic gene sets from Wnt3a-treated versus untreated cells in both the H2030 and PC9 systems, combining the responses in both parental and metastatic derivatives. To obtain a more comprehensive transcriptional readout, we employed approaches based on a correlation coefficient method (Chang et al., 2005; Xu et al., 2008). With this method, the expression trends of many pathway-associated genes can be converted into a continuous score that avoids arbitrary expression level criteria and is applicable across multiple data sets.

When tested in our 107 tumor lung adenocarcinoma cohort, the resulting H2030 and PC9 WNT-responsive gene sets were

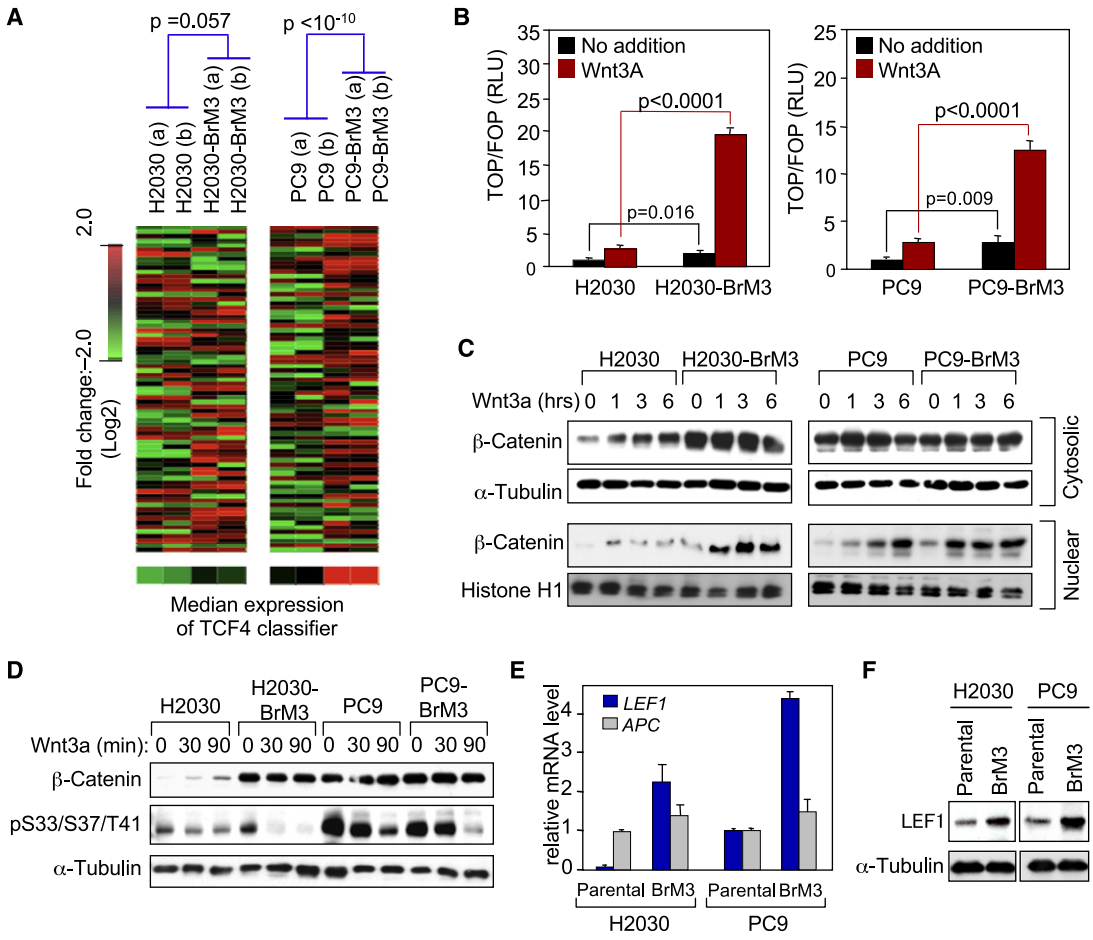

Figure 3. WNT/TCF Activity Is Deregulated in Metastatic Lung Adenocarcinoma Cells

(A) Expression of the TCF4 classifier in duplicate samples (a and b) of the indicated derivatives is presented as a heat map. The bottom row represents the median expression of the TCF4 signature. p values are from a t test comparing median expression.

(B) Normalized luciferase measurements of specific TOP-FLASH over nonspecific FOP-FLASH activity (TOP/FOP RLU), in derivatives that were mock treated or stimulated with recombinant Wnt3A for 12 hr. Error bars represent the SEM. p values are based on a two-sided Student's t test.

(C) Denoted cells were treated with Wnt3a for 0, 1, 3, and 6 hr. Immunoblots were performed for cytosolic (top) or nuclear (bottom) β-catenin, α-tubulin, and histone H1.

(D) Cells were treated with Wnt3a for 0, 30, and 90 min. Overall β-catenin protein levels and its ser33/37/Thr41-phosphorylated form were determined by immunoblot.

(E) Basal expression of *LEF1* and *APC*. Error bars indicate 95% confidence interval from triplicate qRT-PCR samples.

(F) Immunoblot for LEF1 protein.

independently associated with metastatic recurrence to multiple organ sites (Figures S3A and S5B). PC9 and H2030 cells express WNT-responsive genes which only partial overlap. These differences may reflect pathway activation in the context of different tumor developmental histories. To derive a broader WNT/TCF pathway classifier from these two gene sets, we combined probe sets that were regulated by Wnt3a in at least one experimental system with similar expression trends in the other and which were still associated with clinical outcome in MSKCC set 1 (refer to the Experimental Procedures). This yielded a lung cancer WNT gene set (LWS), consisting of 91 probes sets including 81 known genes (Table S2).

The LWS displayed improved prediction of metastatic relapse compared to the TCF4 classifier in the initial cohort of primary lung adenocarcinomas (MSKCC set 1, p = 0.001; Figure 4A) and, notably, in an independent lung adenocarcinoma data set (MSKCC set 2, $p = 9.6 \times 10^{-5}$; Figure 4A) and among lung adenocarcinomas in a cohort of mixed lung tumors (SMC set, p = 0.0025; Figure 4B). The LWS was associated with recurrence in stage I lung adenocarcinomas (Figure 4C), and did not predict metastasis in squamous lung carcinomas (Figure 4B) or in breast carcinomas (Padua et al., 2008) (Figure 4D). Consistent with our model systems, the LWS predicted distant lung adenocarcinoma relapse to both brain and bone (Figures S3C and S3D). Although the H2030-BrM3 or PC9-BrM3 were brain isolates, we were unable to obtain from these cells a common signature that would-predict brain relapse with methods that previously revealed organ-specific metastasis signatures (Bos et al., 2009; Minn

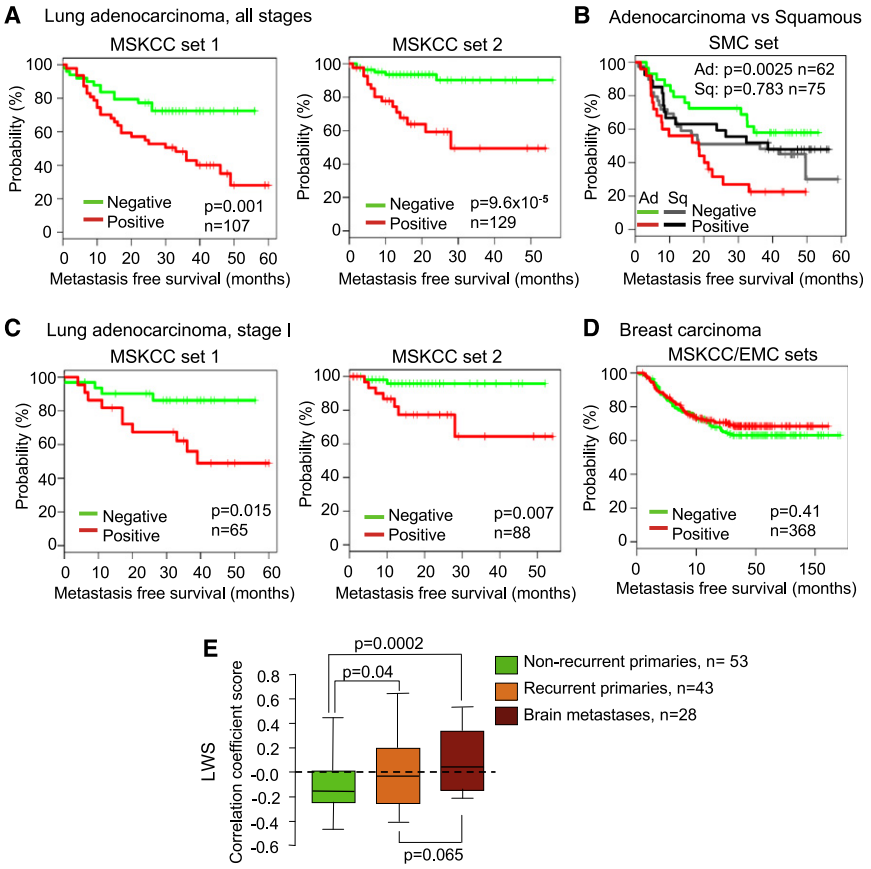

Figure 4. A Specific WNT-Responsive Gene Set Associated with Lung Adenocarcinoma Metastasis

Independent transcriptional predictors from H2030 and PC9 derivatives were obtained by comparison of Wnt3a activated with unstimulated cells and were combined to yield the lung cancer WNT-responsive gene set (LWS).

(A) Kaplan-Meier curves for metastasis-free survival based on LWS expression in MSKCC set 1 and MSKCC set 2. Green, LWS negative; red, LWS positive.

(B) Performance of the LWS in the Samsung Medical Center (SMC) set, including a mix of adenocarcinomas and squamous carcinomas of the lung.

(C) LWS prediction of relapse was observed in stage I lung adenocarcinomas.

(D) Performance of the LWS in a combined MSKCC-EMC cohort of 368 primary breast cancers. A log rank test was used to determine p values in (A)–(D).

(E) The LWS was converted into a Pearson correlation coefficient score that compares the degree of correlation for LWS expression between WNT activated cell lines, primary adenocarcinomas that included clinical annotation within 5 years (43 recurrences and 53 non recurrences), and 28 brain metastases. Data are presented as a Box-whisker plot. p values were calculated by Student's t test.

et al., 2005a). To determine the association of LWS status with overall patient survival, we tested four independent stage I lung adenocarcinoma cohorts from a multi-institutional study (Shedden et al., 2008). In three out of the four cohorts tested, the LWS predicted poor survival in stage I adenocarcinomas (Figures S4A–S4E). Altogether, these results demonstrate an association of WNT hyperactivation with distant multiorgan metastatic potential of lung adenocarcinomas.

By using the LWS in a Pearson correlation coefficient score, we compared brain samples from lung adenocarcinoma patients (n = 28; Figure 4E) to either primary lung adenocarcinomas from patients who remained disease free over 5 years (n = 53) or primary lung adenocarcinomas from patients who recurred in any site (n = 43). Lung adenocarcinoma metastases to bone are rarely resected, and were not available for study. The expression trends of LWS genes in brain metastases resembled more closely primary adenocarcinomas that recurred (Figure 4E). Thus, the activation of WNT/TCF appears to be maintained during brain metastatic progression in clinical samples.

LEF1 and *HOXB9* are WNT/TCF Targets that Mediate Metastasis

To evaluate the functional role of WNT/TCF signaling in lung adenocarcinoma metastasis, we disrupted this pathway by expressing dominant-negative TCFs (dnTCF1 and/or dnTCF4) that lack the N-terminal binding site for β-catenin (van de Wetering et al., 2002). Stable expression of dnTCF4 in H2030-BrM3 cells partially decreased the TCF activity (Figures S5A and S5B) and metastatic activity of these cells (Figure 5A). Coexpression of dnTCF1 and dnTCF4 in PC9-BrM3 cells (Figures S5C and S5D) abated the metastatic activity of these cells in different organs in the same mouse (Figure 5B). Partial reduction in TCF activity had little effect on BrM3 pulmonary growth (Figures 5C and 5D).

To identify specific mediators of WNT prometastatic functions, we focused on a subset of LWS genes whose expression level was strongly correlated with the metastatic potential of our cell derivatives and are implicated in developmental programs. Three genes that fulfilled these criteria were *lymphoid enhancer-binding factor 1* (*LEF1*), *homeobox B9* (*HOXB9*), and *bone morphogenetic protein 4* (*BMP4*). *HOXB9* is a TCF4 target (Hatzis et al., 2008) and belongs to the homeobox transcription factor gene family, which is critical for embryonic segmentation and limb patterning (Abate-Shen, 2002). *LEF1* encodes a transcriptional effector of the canonical WNT pathway and is a target of Wnt3a and TCF4. LEF1 upregulation by WNT may mediate signal amplification during malignancy (Hovanes et al., 2001). *BMP4* belongs to the TGF-β superfamily, can be induced by WNT, and regulates stem cell differentiation and multiple developmental processes (Shu et al., 2005; ten Dijke et al., 2003; Varga and Wrana, 2005).

The expression level of *LEF1* and *HOXB9* was marginal in parental H2030 cells, but was increased and potently induced by Wnt3a in the H2030-BrM3 cells (Figure 5E). In parental PC9

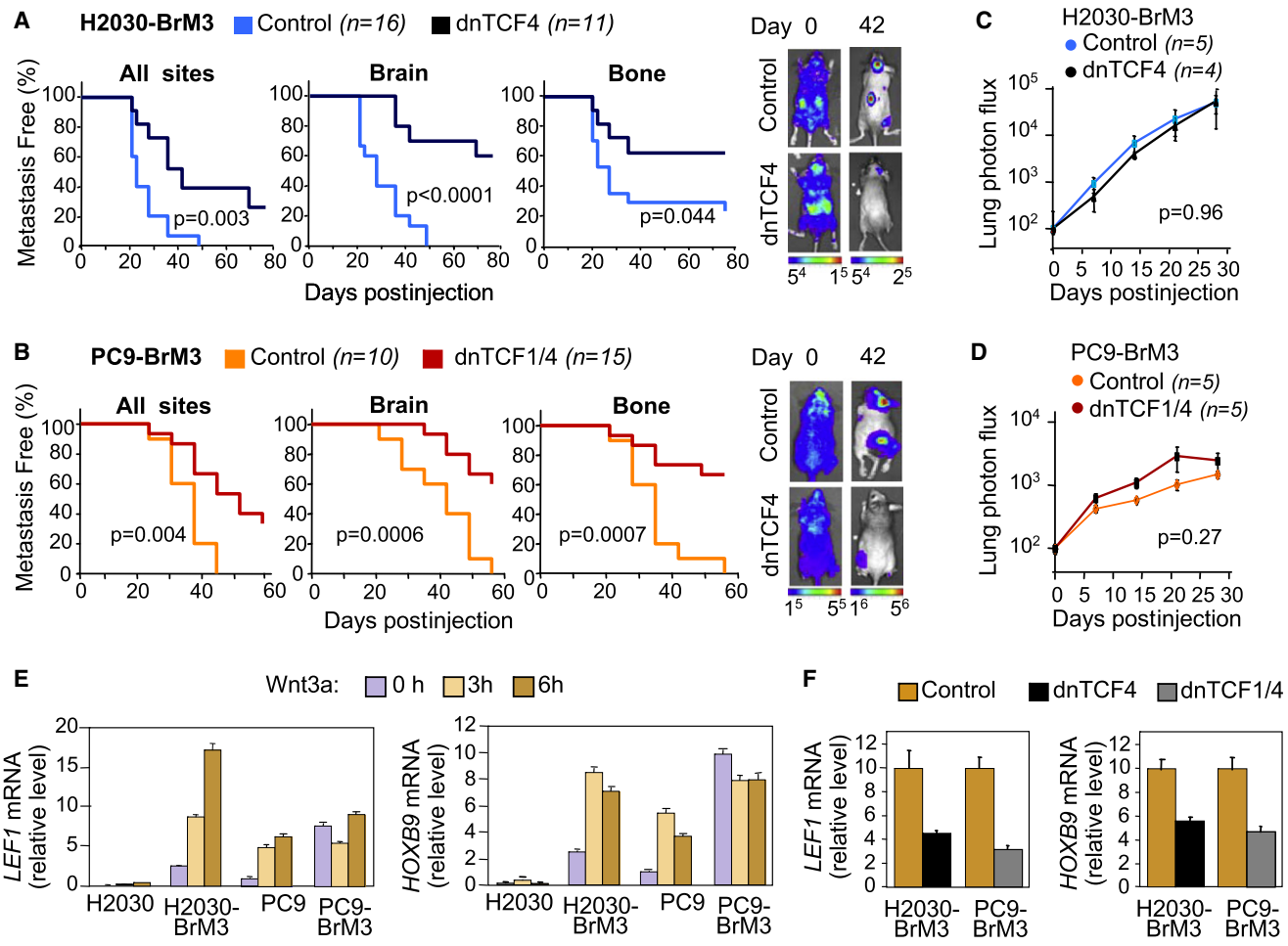

Figure 5. LEF1 and HOXB9 Are Targets of the Metastatic WNT/TCF Pathway

(A) Kaplan-Meier curves for metastasis after inoculation of 5 × 10^4 cells stably expressing an empty vector control or dominant-negative TCF4 (dnTCF4), with representative bioluminescent images.

(B) Control or dnTCF1 and dnTCF4 were expressed in PC9-BrM3 cells. Metastasis was assayed as in (A). p values are based on log rank test.

(C) Lung/pleural tumor growth of H2030-BrM3 cells expressing an empty vector or dnTCF4 as in Figure 2K.

(D) Similar experiments were performed with control and dnTCF1/4-expressing PC9-BrM3 cells. Error bars represent the SEM. p values are based on a two-sided Student's t test.

(E) *LEF1* and *HOXB9* expression were measured via qRT-PCR after Wnt3A stimulation for 0, 3, and 6 hr. Error bars indicate 95% confidence interval from replicates.

(F) The indicated lines were treated with Wnt3A for 3 hr, and levels of *LEF1* and *HOXB9* were determined as in (E).

cells, Wnt3a addition augmented the expression level of *LEF1* and *HOXB9*, whereas these genes were highly expressed and no further inducible by Wnt3a in PC9-BrM3 cells (Figure 5E). Expression of dnTCFs decreased the expression of *LEF1* and *HOXB9* in BrM3 cells (Figure 5F). Thus, the response patterns of *LEF1* and *HOXB9* are consistent with a constitutive hyperactivation of WNT/TCF signaling in PC9 cells and a hypersensitivity to Wnt stimulation in H2030 cells (refer to Figures 3C and 3D).

To achieve specific inhibition of putative WNT/TCF prometastatic genes, we decreased *LEF1* or *HOXB9* by stable RNA interference (RNAi)-mediated knockdown in BrM3 derivatives (Figure S6A). Knockdown of *LEF1* or *HOXB9* significantly decreased the ability of H2030-BrM3 and PC9-BrM3 cells to form bone and brain metastases (Figures 6A and S6B). Knockdown of *BMP4* had no effect on metastasis (data not shown). Reduction of *LEF1* or *HOXB9* did not affect the growth of PC9-BrM3 cells implanted in the lung (Figure S7A). In H2030-BrM3 cells, *HOXB9* knockdown did not affect lung and pleural growth rates, whereas *LEF1* knockdown had a partial inhibitory effect (Figure S7B). These results are consistent with the tumor reinitiating advantage of H2030-BrM3 but not PC9-BrM3 cells over their parental counterparts (refer to Figure S2D). Moreover, overexpression of *LEF1* and *HOXB9* in the parental H2030 and PC9 cell lines increased their metastatic activity from circulation to bone and brain (Figures S8 and 6B–6E). Collectively, these results suggest that *HOXB9* and *LEF1* can enhance the competence of lung adenocarcinoma for brain and bone metastasis.

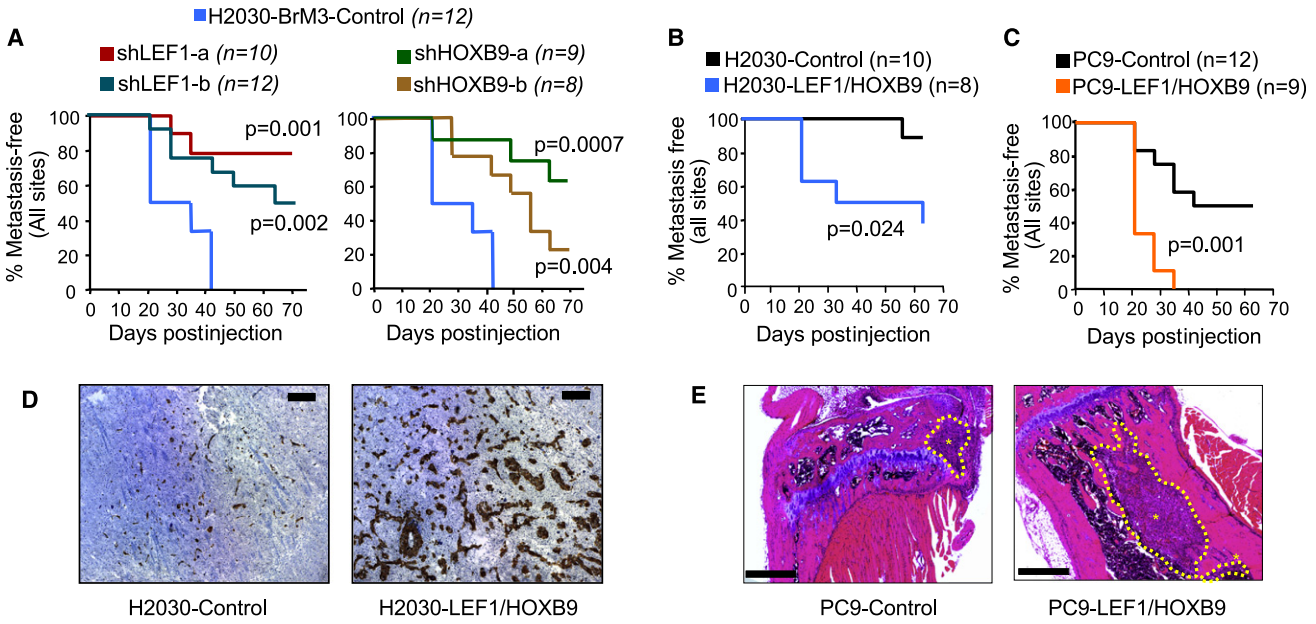

Figure 6. LEF1 and HOXB9 Mediate Metastasis

(A) Kaplan-Meier curves of overall metastasis incidence, for H2030-BrM3 cells encoding control or independent hairpins (sh-a and sh-b) against *LEF1* or *HOXB9*. Left: Metastasis in mice inoculated arterially with H2030-BrM3 control, BrM3-shLEF1-a, or BrM3-shLEF1-b cells. Right: H2030-BrM3 control cells versus shHOXB9-a or shHOXB9-b cells.

(B) H2030 parental cells overexpressing either empty vector control or *LEF1* and *HOXB9* were inoculated at 5×10^4 cells/mouse, and overall metastasis incidence quantified as in (A).

(C) A similar experiment was performed with PC9 parental lines overexpressing empty vector or *LEF1* and *HOXB9*.

(D) Brain tissue from animals inoculated with the indicated lines. Brown, GFP^+ tumor foci. Scale bars represent 200 μm.

(E) Typical hind limbs extracted from animals inoculated with the indicated lines and that had detectable luminescent signal. * indicates bone lesions. Scale bars represent 500 μm. p values are based on log rank test.

LEF1 and HOXB9 as Mediators of Colony Outgrowth and Chemotactic Cell Invasion

The biological properties of LEF1 and HOXB9 were further studied ex vivo with the H2030-BrM3 population, which has a low threshold for exogenous WNT activation. Given the link between WNT/TCF and metastasis to multiple organs, we focused on the general functions of metastatic outgrowth and invasion. Knockdown of *LEF1* and *HOXB9* did not affect general cell viability in monolayer culture (Figures S2A and S2B). However, when cultured in Matrigel, H2030-BrM3 cells formed colonies that grew larger in size (Figure 7A) and in number compared to the parental H2030 cells (Figure 7B, black bars). Wnt3a addition further increased the colony outgrowth (Figure 7B, yellow bars), consistent with the tumor reinitiation advantage of these cells when implanted in the lung. Interestingly, knockdown of *LEF1* expression decreased the size (Figure 7A) and number of the metastatic H2030-BrM3 colonies (Figure 7B), whereas decreasing *HOXB9* expression had no effect.

To analyze metastatic invasion, we measured the infiltration of these cells through Matrigel in a modified Boyden chamber assay (Figure 7C). Parental H2030 and H2030-BrM3 cells showed a similar basal ability to infiltrate Matrigel (Figure 7D). However, given the strong astrocytic reaction elicited at the invasive edge of metastatic lesions in vivo (refer to Figure 2I), we repeated the invasion assays using astrocyte-conditioned media as a source of chemoattractant in the bottom chamber. Under these conditions, the invasive activity of H2030-BrM3 was significantly higher than that of parental cells (Figure 7D). Preincubation of H2030-BrM3 cells with Wnt3a increased their invasion toward stromal conditioned media (Figure 7D, blue bars). Wnt ligand stimulated the invasion of the parental PC9 cells, while PC9-BrM3 cell displayed higher basal invasiveness (Figure S9), consistent with their expression of *LEF1* and *HOXB9*. Wnt3a did not act as a chemoatractant, since invasion was unaffected by the addition of Wnt3a to the bottom chamber (data not shown). Notably, short hairpin RNA (shRNA)-mediated knockdown of either *LEF1* or *HOXB9* inhibited invasion in H2030-BrM3 and PC9-BrM3 cells (Figure 7E). The metastatic potential of BrM3 cells and their responsiveness to WNT activation were not associated with changes in the TCF target *c-myc*, nor were these phenotypes consistently linked to markers of epithelial-mesenchymal transition, such as E-cadherin or vimentin expression (Figure S10).

DISCUSSION

The evidence presented here suggests that a hyperactive WNT/TCF pathway enhances the ability of human lung adenocarcinomas to develop brain and bone metastases. Two WNT target genes, *LEF1* and *HOXB9*, are identified as promoters of lung adenocarcinoma metastasis and mediators of chemotactic invasion and colony outgrowth. These findings provide insights into

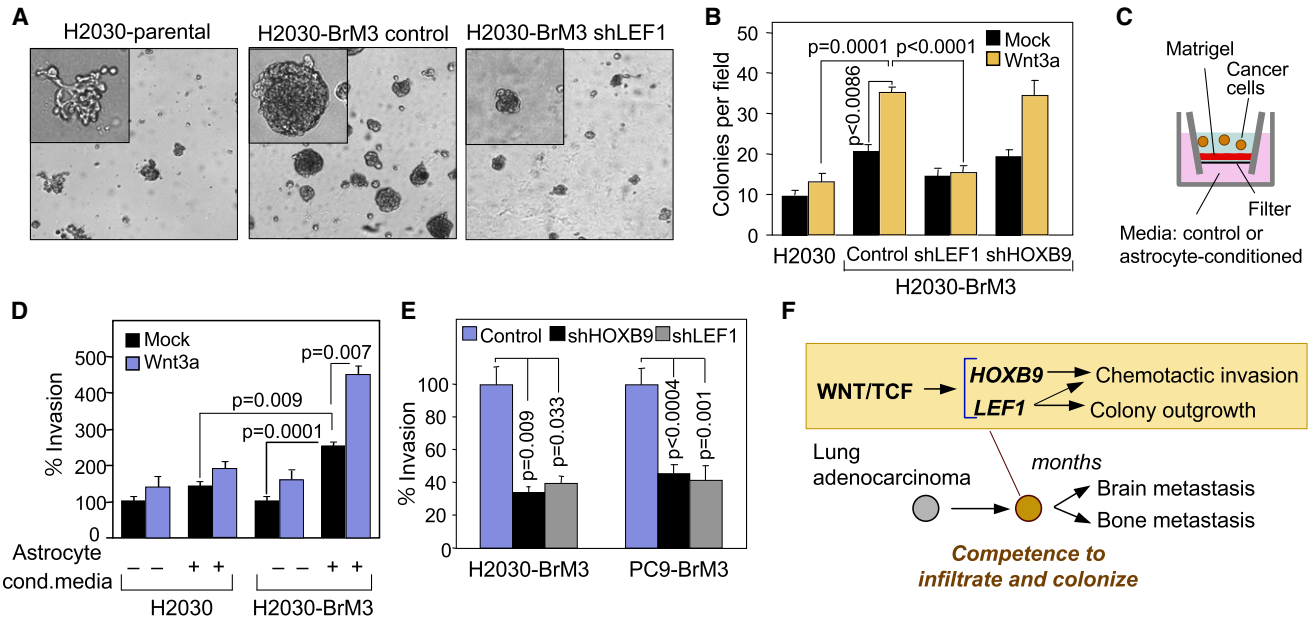

Figure 7. LEF1 and HOXB9 Potentiate Metastatic Outgrowth and Chemotactic Invasion

(A) The indicated lines were plated into Matrigel, and 10× images of colonies were captured after 10 days in serum-containing media, in the presence or absence of Wnt3a. The inset shows representative colonies at 20×.

(B) Quantification of colonies in the absence (black) or presence (yellow) of Wnt3A.

(C) Schematic of invasion assay. Parental and metastatic BrM3 cells were mock (black) or Wnt3a stimulated (blue) and seeded into transwell inserts layered with Matrigel. Assays were performed in the presence of control (–) or astrocyte-conditioned (+)media in the bottom chamber.

(D) Quantification was normalized to the invasion of untreated parental cells.

(E) Cells were stimulated with Wnt3A and used as in (C), with astrocyte chemoattractant. Invasion of the indicated knockdown cells relative to their respective BrM3 control cells is shown. Error bars indicate the SEM. p values were calculated based on a two-sided Student's t test.

(F) Model depicting the roles of LEF1 and HOXB9 within a WNT/TCF program that drives early multiorgan metastasis in lung adenocarcinoma.

the determinants of the typically rapid, multiorgan metastatic progression of this disease.

WNT/TCF Signaling Mediates Lung Adenocarcinoma Metastasis

We derived a lung cancer WNT gene response (LWS) that can identify lung adenocarcinomas with aggressive biological characteristics and poor clinical outcome. WNT/TCF pathway activation as detected by gene expression is associated with metastasis to brain and bones, two prominent sites of distant relapse in lung adenocarcinoma, and distinguishes early stage I lung adenocarcinomas from patients that are most likely to progress in independent cohorts. However, it does not predict relapse in squamous lung carcinoma or breast carcinoma. The transcriptional output of WNT activation is context dependent (Clevers, 2006; Logan and Nusse, 2004), and other WNT components or different pathway combinations may also contribute to lung cancer progression with poor prognosis. Nevertheless, our evidence indicates a unique association between the WNT/TCF pathway and metastatic propensity in human lung adenocarcinomas.

Hyperactivation of WNT/TCF is a uniform property of highly metastatic subpopulations that we obtained from different human lung adenocarcinoma cell lines. These cells lines correspond to two defined subtypes of lung adenocarcinoma—the EGFR and KRAS molecular subtypes. *KRAS* and *EGFR* mutations are present in approximately 25% and 20% of human lung adenocarcinomas, respectively (Rodenhuis et al., 1988; Sharma et al., 2007), and have been validated as oncogenes. However, lung adenocarcinomas initiated by these mutations require additional alterations in order to metastasize to distant sites (Ji et al., 2006; Johnson et al., 2001; Politi et al., 2006). The fact that these cell lines were derived from lymph node samples suggests that the acquisition of a hyperactive WNT/TCF pathway within a subset of malignant cells preceded their colonization of distant organs.

The hyperactivation of WNT/TCF in our model of metastatic lung adenocarcinomas does not correlate with a preponderance of typical somatic mutations in this pathway. Mutations in WNT pathway components are common tumor-initiating events in colorectal and gastric cancers but are less frequent in lung adenocarcinomas (Ding et al., 2008). Deregulation of this pathway may result from additional epigenetic alterations. Interestingly, the silencing of WNT antagonist has been reported in cell lines, as well as tumors from early-stage and relapsing NSCLC patients (Brock et al., 2008; Licchesi et al., 2008; Mazieres et al., 2005). While the diverse mechanisms that regulate the WNT pathway in our models remain to be elucidated, an end result of this process is the elevated expression of at least two transcription factors, *LEF1* and *HOXB9*, that encode different prometastatic functions, some of which are not required for tumor growth in the lung. The activation in primary tumors of

prometastatic functions that provide no local growth advantage is not without precedent (Karnoub et al., 2007; Padua et al., 2008). The hyperactivity of the WNT/TCF pathway in lung adenocarcinomas observed here might reflect a presence of Wnt ligands in the primary tumor stroma, a feature of the tumor cell of origin, an epigenetic bystander alteration of WNT/TCF pathway components, or a combination of these mechanisms.

LEF1 and HOXB9 Are Effectors of the WNT Metastasis Program

LEF1 and *HOXB9* are direct transcriptional targets of the TCF4 transcription factor (Hatzis et al., 2008). HOXB9 is part of a homeobox family gene cluster whose expression is normally restricted to embryogenesis (Abate-Shen, 2002). HOXB9 expression has been reported in lung cancer cell lines (Calvo et al., 2000), but its function is unknown. LEF1 is a prototypical transcriptional mediator of WNT gene response, and its activation may amplify pathological WNT signaling (Hovanes et al., 2001). Moreover, LEF1 can interact with cofactors independently of β-catenin (Arce et al., 2006). High basal levels of *LEF1* in metastatic cells may increase transcriptional activation without additional changes in β-catenin.

In our lung adenocarcinoma model, WNT/TCF hyperactivation can stimulate bone and brain metastasis independently of changes in intrinsic tumor cell viability or of a general growth advantage. We show that HOXB9 and LEF1 increase cancer cell invasion and that LEF1 promotes tumor colony outgrowth in extracellular matrix. Interestingly, the phenotype of our metastatic derivatives resembles that described for bronchioalveolar stem cells (BASCs) (Kim et al., 2005), which exhibit enhanced WNT activity after injury (Zhang et al., 2008). Thus, HOXB9 and LEF1 may fulfill progenitor cell functions that are reenacted during metastatic progression. The stem cell reprogramming gene c-*MYC* is a target of the LEF/TCF pathway in colon cancer cells (He et al., 1998) but does not correlate with the metastatic potential of the lung adenocarcinoma lines studied here. However, we do not exclude the possible involvement of other WNT target genes in lung adenocarcinoma metastasis.

Early Metastatic Competence versus Progressive Metastatic Speciation

The present findings illuminate a central concept in lung adenocarcinoma progression, namely, the role of a prometastatic signal that is gradually increased in primary tumors and enables their rapid metastatic spread. Unlike breast or prostate cancer metastasis, which may develop years to decades after the removal of a primary tumor, lung adenocarcinomas are typically competent to metastasize rapidly to multiple organs. The long latency of metastasis in breast or prostate carcinoma implies the need for further malignant evolution of the disseminated cancer cells in the infiltrated organs. In contrast to the protracted evolution of cancers which undergo long periods of remission before clinical metastasis, the short latency of relapse in lung adenocarcinomas predicts their acquisition of a prometastatic program early on and a lesser degree of organ speciation. Our identification of a mechanism that provides overall metastatic competence in early stage lung adenocarcinomas is in agreement with these predictions.

Intracranial relapses are a significant source of failure after treatments with chemotherapy (Chen et al., 2007) and targeted drugs (Omuro et al., 2005). While animal models of lung cancer represent a critical venue to address this problem, genetically modified mouse models of lung cancer reported to date yield metastatic tumors that occur in visceral organs but not in the brain (Jackson et al., 2005; Zheng et al., 2007). While not without limitations, our experimental systems recapitulate important phenotypic and molecular features of lung adenocarcinoma, including brain and bone metastasis, and a hyperactive WNT/TCF pathway in the background of relevant oncogenic mutations. This model may be useful for achieving a deeper understanding of early metastatic events and the development of improved treatments for lung adenocarcinoma patients at risk for metastasis.

EXPERIMENTAL PROCEDURES

Additional methods for cell culture, in vivo selection, in vitro assays, immunostaining procedures, retroviral shRNA targets, sequencing, and gene expression analysis are provided in the Supplemental Data.

Animal Studies

Animal procedures were in accordance with the MSKCC Institutional Animal Care and Use Committee. Xenografts were performed on mice with SCID mutation in a nonobese diabetic background (NOD.SCID) or on mice carrying the nude mutation crossed to the CBA/N X chromosome-linked immune defect and beige mutations (bg-nu-Xid). Animals were aged matched between 4 and 6 weeks. NSCLC cell lines were engineered to stably express a triple modality vector encoding *GFP-luciferase* fusion (Minn et al., 2005b). For experimental metastasis assays, between 10^4 and 10^5 cells were resuspended in 0.1 ml PBS and injected into the right ventricle. Metastasis was detected by bioluminescence with an IVIS 200 Xenogen and confirmed by X-ray, MRI, and/or histology. Incidence of metastasis was quantified on the basis of the luminescent signal in limbs and/or brain at a given time point and presented as Kaplan-Meir curves. For lung tumorigenesis, 10^4 cells were resuspended in a 1:2 mixture of PBS and growth factor-reduced Matrigel (BD Biosciences) and injected into the lung through the left rib cage of mice as previously described (Doki et al., 1999). Alternatively, cells were injected into the lateral tail vein. Growth rate in the lung/pleura was measured as a function of lung photon flux normalized to day 0 in live animals. Tumorigenic growth rates were similar when implanted subcutaneously. Metastasis phenotype was independent of animal sex.

LEF/TCF Reporter Assays

The TOP-Flash and FOP-Flash promoters were subcloned into pGL4.82-Renilla luciferase constructs (Promega). Cells were transfected with Lipofectamine 2000 and selected for 2 days in puromicin. Transfected cell were then reseeded into 24 well plates at 50,000 cells/well before treatment with recombinant Wnt3a (50−100 ng/ml; R&D Systems) for 12 hr. Reporter assays were performed according to the manufacturer's instructions (Promega). Promoter activity was calculated as the ratio of specific TOP-Flash over nonspecific FOP-Flash relative renilla luciferase units (RLU).

Gene Expression Profiling

Subconfluent parental and metastatic derivatives were serum starved overnight and either mock treated or stimulated with recombinant Wnt3A (75–100 ng/ml) for 3 hr. RNA was extracted from duplicate samples of each condition using the RNeasy mini kit (QIAGEN). Labeling and hybridization of the cell line samples to the HG-U133A_2 gene expression chip (Affymetrix) was performed by the MSKCC Genomics Core Facility. Microarray data from a cohort of 107 lung adenocarcinoma tumors (MSKCC set 1), a second cohort of 129 adenocarcinomas (MSKCC set 2) including tumors from Chitale et al. (2009), and 28 brain metastasis were analyzed on Affymetrix HG-U133A and HG-U133A_2 platforms. A third data set containing a mix of

lung adenocarcinomas and squamous carcinomas from the Samsung Medical Center (SMC set; HG-U133A Plus 2.0) was publicly available. For pathway and correlation coefficient analysis, raw CEL data were preprocessed with RMA algorithm implemented by the *affy* package of *R* statistical software (designated as *R* hereafter). Gene expression data of cell derivatives are deposited at GEO (GSE14107). Samsung Medical Center set was obtained from GEO (GSE8894). Raw data and clinical annotation for MSKCC sets 1, 2, and brain metastasis are available at http://cbio.mskcc.org/Public/lung_array_data/.

Pathway Signature Derivation

Genes regulated by KRAS and dnTCF4 were extracted from published results (Sweet-Cordero et al., 2005; van de Wetering et al., 2002) and matched to the corresponding Affymetrix probes (HG-U133A platform). The Affymetrix version of the TCF4 signature was used to cluster MSKCC set 1 in an unsupervised manner (by the "*heatmap.2*" function of "*gplots*" package of *R*). The cluster that overexpresses the majority of dnTCF4 genes was defined as TCF4+, and the other cluster was defined as TCF4−. The clinical outcomes of the two clusters were compared by log-rank test with the "*survdiff*" function of "*survival*" package of *R*. β-catenin, c-*myc*, SRC, E2F3, and TGF-β gene lists were obtained from previous results (Bild et al., 2006; Padua et al., 2008) and used for unsupervised analysis.

Derivation and Characterization of a Lung Cancer WNT Gene Response Set

A combinatory approach based on correlation coefficient score and unsupervised clustering was used to evaluate the association between Wnt3A-mediated gene responses in lung adenocarincoma cell lines and relapse in MSKCC sets 1, 2, and SMC lung adenocarcinoma clinical cohorts. This was confirmed by pathway meta-analysis. A comprehensive description of these methods is provided in the Supplemental Data.

SUPPLEMENTAL DATA

Supplemental Data include Supplemental Experimental Procedures, two tables, ten figures, and video summary and can be found with this article online at http://www.cell.com/supplemental/S0092-8674(09)00455-3.

ACKNOWLEDGMENTS

We would like to express deep gratitude to our late colleague William L. Gerald. We are indebted to H. Varmus, W. Pao, V. Rusch, and members of the Massagué laboratory for insightful discussions. We thank A. Heguy for supervising sequencing and mutational analysis. H. Clevers, E. Batlle, R. Moon, W. Pao, and H. Varmus generously provided constructs and cell lines. This work was supported by the Alan and Sandra Gerry Metastasis Research Initiative and National Institutes of Health grant P01-129243 (M.G.K., M.L., W.L.G., and J.M.). D.X.N. was the Bayer postdoctoral fellow of the Damon Runyon Cancer Research Foundation. A.C.C. was supported by an American Society of Clinical Oncology Career Development Award. J.M. is an Investigator of the Howard Hughes Medical Institute.

Received: August 4, 2008
Revised: December 12, 2008
Accepted: April 7, 2009
Published online: July 2, 2009

REFERENCES

Abate-Shen, C. (2002). Deregulated homeobox gene expression in cancer: cause or consequence? Nat. Rev. Cancer *2*, 777–785.

Arce, L., Yokoyama, N.N., and Waterman, M.L. (2006). Diversity of LEF/TCF action in development and disease. Oncogene *25*, 7492–7504.

Bild, A.H., Yao, G., Chang, J.T., Wang, Q., Potti, A., Chasse, D., Joshi, M.B., Harpole, D., Lancaster, J.M., Berchuck, A., et al. (2006). Oncogenic pathway signatures in human cancers as a guide to targeted therapies. Nature *439*, 353–357.

Bos, P.D., Zhang, X.H.F., Nadal, C., Shu, W., Gomis, R.R., Nguyen, D.X., Minn, A.J., Van de Vijver, M., Gerald, W.L., Foekens, J.A., et al. (2009). Genes that mediate breast cancer metastasis to the brain. Nature, in press. Published online May 6, 2009. 10.1038/nature08021.

Brock, M.V., Hooker, C.M., Ota-Machida, E., Han, Y., Guo, M., Ames, S., Glockner, S., Piantadosi, S., Gabrielson, E., Pridham, G., et al. (2008). DNA methylation markers and early recurrence in stage I lung cancer. N. Engl. J. Med. *358*, 1118–1128.

Calvo, R., West, J., Franklin, W., Erickson, P., Bemis, L., Li, E., Helfrich, B., Bunn, P., Roche, J., Brambilla, E., et al. (2000). Altered HOX and WNT7A expression in human lung cancer. Proc. Natl. Acad. Sci. USA *97*, 12776–12781.

Chang, H.Y., Nuyten, D.S., Sneddon, J.B., Hastie, T., Tibshirani, R., Sorlie, T., Dai, H., He, Y.D., van't Veer, L.J., Bartelink, H., et al. (2005). Robustness, scalability, and integration of a wound-response gene expression signature in predicting breast cancer survival. Proc. Natl. Acad. Sci. USA *102*, 3738–3743.

Chen, A.M., Jahan, T.M., Jablons, D.M., Garcia, J., and Larson, D.A. (2007). Risk of cerebral metastases and neurological death after pathological complete response to neoadjuvant therapy for locally advanced nonsmall-cell lung cancer: clinical implications for the subsequent management of the brain. Cancer *109*, 1668–1675.

Chitale, D., Gong, Y., Taylor, B., Broderick, S., Brennan, C., Somwar, R., Golas, B., Wang, L., Motoi, N., Szoke, J., et al. (2009). An integrated genomic analysis of lung cancer reveals loss of DUSP4 in EGFR-mutant tumors. Oncogene, in press. Published online June 15, 2009. 10.1038/onc.2009.135.

Clevers, H. (2006). Wnt/beta-catenin signaling in development and disease. Cell *127*, 469–480.

Ding, L., Getz, G., Wheeler, D.A., Mardis, E.R., McLellan, M.D., Cibulskis, K., Sougnez, C., Greulich, H., Muzny, D.M., Morgan, M.B., et al. (2008). Somatic mutations affect key pathways in lung adenocarcinoma. Nature *455*, 1069–1075.

Doki, Y., Murakami, K., Yamaura, T., Sugiyama, S., Misaki, T., and Saiki, I. (1999). Mediastinal lymph node metastasis model by orthotopic intrapulmonary implantation of Lewis lung carcinoma cells in mice. Br. J. Cancer *79*, 1121–1126.

Feld, R., Rubinstein, L.V., and Weisenberger, T.H. (1984). Sites of recurrence in resected stage I non-small-cell lung cancer: a guide for future studies. J. Clin. Oncol. *2*, 1352–1358.

Gaspar, L.E. (2004). Brain metastases in lung cancer. Expert Rev. Anticancer Ther. *4*, 259–270.

Gavrilovic, I.T., and Posner, J.B. (2005). Brain metastases: epidemiology and pathophysiology. J. Neurooncol. *75*, 5–14.

Gottardi, C.J., and Gumbiner, B.M. (2004). Distinct molecular forms of beta-catenin are targeted to adhesive or transcriptional complexes. J. Cell Biol. *167*, 339–349.

Hatzis, P., van der Flier, L.G., van Driel, M.A., Guryev, V., Nielsen, F., Denissov, S., Nijman, I.J., Koster, J., Santo, E.E., Welboren, W., et al. (2008). Genome-wide pattern of TCF7L2/TCF4 chromatin occupancy in colorectal cancer cells. Mol. Cell. Biol. *28*, 2732–2744.

He, T.C., Sparks, A.B., Rago, C., Hermeking, H., Zawel, L., da Costa, L.T., Morin, P.J., Vogelstein, B., and Kinzler, K.W. (1998). Identification of c-MYC as a target of the APC pathway. Science *281*, 1509–1512.

Hess, K.R., Varadhachary, G.R., Taylor, S.H., Wei, W., Raber, M.N., Lenzi, R., and Abbruzzese, J.L. (2006). Metastatic patterns in adenocarcinoma. Cancer *106*, 1624–1633.

Hoffman, P.C., Mauer, A.M., and Vokes, E.E. (2000). Lung cancer. Lancet *355*, 479–485.

Hovanes, K., Li, T.W., Munguia, J.E., Truong, T., Milovanovic, T., Lawrence Marsh, J., Holcombe, R.F., and Waterman, M.L. (2001). Beta-catenin-sensitive isoforms of lymphoid enhancer factor-1 are selectively expressed in colon cancer. Nat. Genet. *28*, 53–57.

Husemann, Y., Geigl, J.B., Schubert, F., Musiani, P., Meyer, M., Burghart, E., Forni, G., Eils, R., Fehm, T., Riethmuller, G., et al. (2008). Systemic spread is an early step in breast cancer. Cancer Cell *13*, 58–68.

Jackson, E.L., Olive, K.P., Tuveson, D.A., Bronson, R., Crowley, D., Brown, M., and Jacks, T. (2005). The differential effects of mutant p53 alleles on advanced murine lung cancer. Cancer Res. *65*, 10280–10288.

Ji, H., Li, D., Chen, L., Shimamura, T., Kobayashi, S., McNamara, K., Mahmood, U., Mitchell, A., Sun, Y., Al-Hashem, R., et al. (2006). The impact of human EGFR kinase domain mutations on lung tumorigenesis and in vivo sensitivity to EGFR-targeted therapies. Cancer Cell *9*, 485–495.

Johnson, L., Mercer, K., Greenbaum, D., Bronson, R.T., Crowley, D., Tuveson, D.A., and Jacks, T. (2001). Somatic activation of the K-ras oncogene causes early onset lung cancer in mice. Nature *410*, 1111–1116.

Karnoub, A.E., Dash, A.B., Vo, A.P., Sullivan, A., Brooks, M.W., Bell, G.W., Richardson, A.L., Polyak, K., Tubo, R., and Weinberg, R.A. (2007). Mesenchymal stem cells within tumour stroma promote breast cancer metastasis. Nature *449*, 557–563.

Karrison, T.G., Ferguson, D.J., and Meier, P. (1999). Dormancy of mammary carcinoma after mastectomy. J. Natl. Cancer Inst. *91*, 80–85.

Kim, C.F., Jackson, E.L., Woolfenden, A.E., Lawrence, S., Babar, I., Vogel, S., Crowley, D., Bronson, R.T., and Jacks, T. (2005). Identification of bronchioalveolar stem cells in normal lung and lung cancer. Cell *121*, 823–835.

Klaus, A., and Birchmeier, W. (2008). Wnt signalling and its impact on development and cancer. Nat. Rev. Cancer *8*, 387–398.

Klein, C.A., Schmidt-Kittler, O., Schardt, J.A., Pantel, K., Speicher, M.R., and Riethmuller, G. (1999). Comparative genomic hybridization, loss of heterozygosity, and DNA sequence analysis of single cells. Proc. Natl. Acad. Sci. USA *96*, 4494–4499.

Koizumi, F., Shimoyama, T., Taguchi, F., Saijo, N., and Nishio, K. (2005). Establishment of a human non-small cell lung cancer cell line resistant to gefitinib. Int. J. Cancer *116*, 36–44.

Korinek, V., Barker, N., Morin, P.J., van Wichen, D., de Weger, R., Kinzler, K.W., Vogelstein, B., and Clevers, H. (1997). Constitutive transcriptional activation by a beta-catenin-Tcf complex in APC−/− colon carcinoma. Science *275*, 1784–1787.

Licchesi, J.D., Westra, W.H., Hooker, C.M., Machida, E.O., Baylin, S.B., and Herman, J.G. (2008). Epigenetic alteration of Wnt pathway antagonists in progressive glandular neoplasia of the lung. Carcinogenesis *29*, 895–904.

Logan, C.Y., and Nusse, R. (2004). The Wnt signaling pathway in development and disease. Annu. Rev. Cell Dev. Biol. *20*, 781–810.

Martini, N., Bains, M.S., Burt, M.E., Zakowski, M.F., McCormack, P., Rusch, V.W., and Ginsberg, R.J. (1995). Incidence of local recurrence and second primary tumors in resected stage I lung cancer. J. Thorac. Cardiovasc. Surg. *109*, 120–129.

Mazieres, J., He, B., You, L., Xu, Z., and Jablons, D.M. (2005). Wnt signaling in lung cancer. Cancer Lett. *222*, 1–10.

Minn, A.J., Gupta, G.P., Siegel, P.M., Bos, P.D., Shu, W., Giri, D.D., Viale, A., Olshen, A.B., Gerald, W.L., and Massagué, J. (2005a). Genes that mediate breast cancer metastasis to lung. Nature *436*, 518–524.

Minn, A.J., Kang, Y., Serganova, I., Gupta, G.P., Giri, D.D., Doubrovin, M., Ponomarev, V., Gerald, W.L., Blasberg, R., and Massagué, J. (2005b). Distinct organ-specific metastatic potential of individual breast cancer cells and primary tumors. J. Clin. Invest. *115*, 44–55.

Moon, R.T., Kohn, A.D., De Ferrari, G.V., and Kaykas, A. (2004). WNT and beta-catenin signalling: diseases and therapies. Nat. Rev. Genet. *5*, 691–701.

Morin, P.J., Sparks, A.B., Korinek, V., Barker, N., Clevers, H., Vogelstein, B., and Kinzler, K.W. (1997). Activation of beta-catenin-Tcf signaling in colon cancer by mutations in beta-catenin or APC. Science *275*, 1787–1790.

Nguyen, D.X., Bos, P.D., and Massagué, J. (2009). Metastasis: from dissemination to organ-specific colonization. Nat. Rev. Cancer *9*, 274–284.

Omuro, A.M., Kris, M.G., Miller, V.A., Franceschi, E., Shah, N., Milton, D.T., and Abrey, L.E. (2005). High incidence of disease recurrence in the brain and leptomeninges in patients with nonsmall cell lung carcinoma after response to gefitinib. Cancer *103*, 2344–2348.

Padua, D., Zhang, X.H., Wang, Q., Nadal, C., Gerald, W.L., Gomis, R.R., and Massagué, J. (2008). TGFbeta primes breast tumors for lung metastasis seeding through angiopoietin-like 4. Cell *133*, 66–77.

Phelps, R.M., Johnson, B.E., Ihde, D.C., Gazdar, A.F., Carbone, D.P., McClintock, P.R., Linnoila, R.I., Matthews, M.J., Bunn, P.A., Jr., Carney, D., et al. (1996). NCI-Navy Medical Oncology Branch cell line data base. J. Cell. Biochem. Suppl. *24*, 32–91.

Polakis, P. (2007). The many ways of Wnt in cancer. Curr. Opin. Genet. Dev. *17*, 45–51.

Politi, K., Zakowski, M.F., Fan, P.D., Schonfeld, E.A., Pao, W., and Varmus, H.E. (2006). Lung adenocarcinomas induced in mice by mutant EGF receptors found in human lung cancers respond to a tyrosine kinase inhibitor or to down-regulation of the receptors. Genes Dev. *20*, 1496–1510.

Rodenhuis, S., Slebos, R.J., Boot, A.J., Evers, S.G., Mooi, W.J., Wagenaar, S.S., van Bodegom, P.C., and Bos, J.L. (1988). Incidence and possible clinical significance of K-ras oncogene activation in adenocarcinoma of the human lung. Cancer Res. *48*, 5738–5741.

Sasaki, Y., Shinkai, T., Eguchi, K., Tamura, T., Ohe, Y., Ohmori, T., and Saijo, N. (1991). Prediction of the antitumor activity of new platinum analogs based on their ex vivo pharmacodynamics as determined by bioassay. Cancer Chemother. Pharmacol. *27*, 263–270.

Schmidt-Kittler, O., Ragg, T., Daskalakis, A., Granzow, M., Ahr, A., Blankenstein, T.J., Kaufmann, M., Diebold, J., Arnholdt, H., Muller, P., et al. (2003). From latent disseminated cells to overt metastasis: genetic analysis of systemic breast cancer progression. Proc. Natl. Acad. Sci. USA *100*, 7737–7742.

Sharma, S.V., Bell, D.W., Settleman, J., and Haber, D.A. (2007). Epidermal growth factor receptor mutations in lung cancer. Nat. Rev. Cancer *7*, 169–181.

Shedden, K., Taylor, J.M., Enkemann, S.A., Tsao, M.S., Yeatman, T.J., Gerald, W.L., Eschrich, S., Jurisica, I., Giordano, T.J., Misek, D.E., et al. (2008). Gene expression-based survival prediction in lung adenocarcinoma: a multi-site, blinded validation study. Nat. Med. *14*, 822–827.

Shu, W., Guttentag, S., Wang, Z., Andl, T., Ballard, P., Lu, M.M., Piccolo, S., Birchmeier, W., Whitsett, J.A., Millar, S.E., et al. (2005). Wnt/beta-catenin signaling acts upstream of N-myc, BMP4, and FGF signaling to regulate proximal-distal patterning in the lung. Dev. Biol. *283*, 226–239.

Sweet-Cordero, A., Mukherjee, S., Subramanian, A., You, H., Roix, J.J., Ladd-Acosta, C., Mesirov, J., Golub, T.R., and Jacks, T. (2005). An oncogenic KRAS2 expression signature identified by cross-species gene-expression analysis. Nat. Genet. *37*, 48–55.

ten Dijke, P., Korchynskyi, O., Valdimarsdottir, G., and Goumans, M.J. (2003). Controlling cell fate by bone morphogenetic protein receptors. Mol. Cell. Endocrinol. *211*, 105–113.

Thomas, A.J., Rock, J.P., Johnson, C.C., Weiss, L., Jacobsen, G., and Rosenblum, M.L. (2000). Survival of patients with synchronous brain metastases: an epidemiological study in southeastern Michigan. J. Neurosurg. *93*, 927–931.

van de Wetering, M., Sancho, E., Verweij, C., de Lau, W., Oving, I., Hurlstone, A., van der Horn, K., Batlle, E., Coudreuse, D., Haramis, A.P., et al. (2002). The beta-catenin/TCF-4 complex imposes a crypt progenitor phenotype on colorectal cancer cells. Cell *111*, 241–250.

Varga, A.C., and Wrana, J.L. (2005). The disparate role of BMP in stem cell biology. Oncogene *24*, 5713–5721.

Xu, L., Shen, S.S., Hoshida, Y., Subramanian, A., Ross, K., Brunet, J.P., Wagner, S.N., Ramaswamy, S., Mesirov, J.P., and Hynes, R.O. (2008). Gene expression changes in an animal melanoma model correlate with aggressiveness of human melanoma metastases. Mol. Cancer Res. *6*, 760–769.

Zhang, Y., Goss, A.M., Cohen, E.D., Kadzik, R., Lepore, J.J., Muthukumaraswamy, K., Yang, J., DeMayo, F.J., Whitsett, J.A., Parmacek, M.S., et al. (2008). A Gata6-Wnt pathway required for epithelial stem cell development and airway regeneration. Nat. Genet. *40*, 862–870.

Zheng, S., El-Naggar, A.K., Kim, E.S., Kurie, J.M., and Lozano, G. (2007). A genetic mouse model for metastatic lung cancer with gender differences in survival. Oncogene *26*, 6896–6904.

Cell, Volume *138*

Supplemental Data

WNT/TCF Signaling through LEF1 and HOXB9 Mediates Lung Adenocarcinoma Metastasis

Don X. Nguyen, Anne C. Chiang, Xiang H.F. Zhang, Juliet Y. Kim, Mark G. Kris, Marc Ladanyi, William L. Gerald, and Joan Massagué

Supplemental Experimental Procedures

Cell culture. NCI-H2030, PC9, and their metastatic derivatives were cultured in RPMI with 10% FBS, glutamine, penicillin, streptomycin, and fungizone. C8S murine astrocyte cell line (ATCC) was cultured in DMEM containing 10% FBS supplemented with penicillin, streptomycin, fungizone, and sodium bicarbonate. The amphotropic retroviral packaging cell line GPG29, expressing VSVG envelop protein under doxycycline mediated repression, was maintained in DMEM containing 10% FBS supplemented with puromycin, G418, doxycycline, penicillin, streptomycin, and fungizone.

***In vivo* selection of metastatic derivatives.** Metastatic derivatives were obtained following the injection of 10^5 cells of either the NCI-H2030 or PC9 cell lines. Bone and brain metastasis were first detected in animals by bioluminescence after 3-6 months and confirmed by X-Ray and magnetic resonance imaging (MRI) respectively. Lesions were extracted from brain. Tissue was minced and placed in warm RPMI medium containing a mixture of 0.125% collagenase III and 0.1% hyaluronidase. Samples were incubated at room temperature for 2 hours with gentle rocking. Cells were then briefly centrifuged, resuspended in 0.25% trypsin, and incubated for an additional 20 min at 37°C, vortexing every 5 min. Cells were resuspended in culture medium and allowed to grow to confluence in a T25 flask. GFP^+ cells were sorted, expanded in culture and re-injected into mice. This process was repeated for three cycles to obtain 3rd generation BrM3 derivatives.

Immunostaining. Mice were sacrificed and perfused with PBS and 4% paraformaldehyde through the left ventricle, before tissues were extracted, fixed, and paraffin-embedded. Brightfield images were collected using an Axioplan2 microscopy system (Zeiss). For immunofluorescence, tumors were fixed and frozen in OCT. Images were captured with a Leica TCS SP2 (DMRXA2) and processed with Volocity (Improvision). Markers of vessels, astrocytes, tumor proliferation, and astrocytes proliferation were identified by staining with antibodies against CD31 (BD Biosciences Pharmingen), GFAP (Dakko), human Ki67 (Pharmingen), and murine Ki67 (Dakko) respectively, followed by fluorescently conjugated secondary antibodies (Jackson Immunoresearch).

Immunoblot. Cells were washed with PBS and lysed using the cytosolic/nuclear fractionation NE-PER kit (Pierce). Proteins were separated by SDS-PAGE, transferred to Nitrocellulose membranes (Bio-Rad), and blotted with antibodies recognizing: ß-catenin (Cell Signaling), phospho-specific ß-catenin (Cell Signaling), LEF1 (Abcam), c-myc (Cell Signaling), E-cadherin (Santa-Cruz), vimentin (NeoMarkers), N-cadherin (Cell signaling), α-tubulin (Sigma), Histone H1 (Cell signaling), and HRP-Conjugated secondary antibodies (Pierce).

Generation of retrovirus. Ha tagged version of dnTCF1 or 4, LEF1, and HOXB9 cDNAs were subcloned into the pBabe retroviral backbone. For knockdown, the following sequences were targeted: 5'- GAGTTATTCCGGGTACATA -3' (shLEF-a), 5'- GTTGCTGAGTGTACTCTAA -3'

(shLEF1-b), 5'- CAGACATCCACACACAGTA -3' (shHOXB9-a), and 5'- CTCCTAGTATGCCCTGTAA -3' (shHOXB9-b). These were cloned into a modified pSM2 mir based vector, which expresses the short hairpin embedded in a larger microRNA sequence (Silva et al., 2005). 40 μg of retroviral-based vectors were transfected into GPG29 cells using Lipofectamine 2000 (Invitrogen). Post-transfection, cells were cultured in DMEM containing 10% FBS and sodium pyruvate, in the absence of doxycycline. Viruses were harvested 48 and 72 hours after transfection, filtered, and concentrated by ultracentrifugation. Concentrated retrovirus was used to infect cells in the presence of 8μg/mL polybrene and infected cells were selected with puromycin. For combination over-expression, retrovirus was used to super-infect previously generated cells and subsequently selected with hygromycin.

***In vitro* growth and cell viability.** 5000 cells of each line were seeded into 12 well plates and cultured under normal monolayer conditions. Samples were lysed at the indicated time points and cell numbers measured as a function of luciferase activity. The viability in response to growth factor deprivation was measured after 5 days in media with 0.2% FBS, using Resazurin (R&D systems) according to the manufacturer's instructions.

Colony growth in Matrigel. Cells were either plated onto 2 well chamber slides (5000 cells/chamber) or 24 well plates (2000 cells/well) coated with a thin layer of growth factor reduced Matrigel. Cells were overlayed with 15% Matrigel and cultured in serum containing media with or without 100 ng/ml of Wnt3A for 10 days. Wnt3A was replenished every two days. Colonies were counted using an inverted microscope. Quantification was based on counts at 10X, from 8-10 independent fields per condition.

Invasion assays. C8S murine astrocytes were plated and allowed to grow to confluence. Astrocytes were conditioned in 0.2% FBS containing RPMI for 48 hours. Sub-confluent tumor cells were pulsed with 5μm cell tracker green™ (Invitrogen) for 30 minutes before being conditioned overnight in 0.2% FBS containing RPMI. The next day, Matrigel coated trans-well inserts with 8um pores (BD biosciences) were placed in control or astrocytes-conditioned media. 25,000-50,000 tumor cells were mock treated or treated with 100ng/ml of recombinant Wnt3a for 6 hours, seeded into trans-wells and fixed in 4% paraformaldehyde after 8-10 hours. Cells on the apical side of inserts were scraped off and the trans-well membrane mounted onto slides. Invasion to the basolateral side of the membrane was visualized with a Zeiss Axioplan2 immunofluorescent microscope at 10X. Pictures of 6-10 random fields across three replicate wells were captured for quantification using Image J software (NIH). In general, 50-150 counts/field of PC9 or H2030 cells invade through Matrigel. Invasion of the indicated lines was plotted as a fold difference compared to either parental or control BrM3 cells.

mRNA levels. 250 ng of total RNA was used in a reverse transcriptase reaction with the SuperScript III first-strand synthesis system (Invitrogen). Quantitative PCR included four replicates per cDNA sample. Human *LEF-1*, *HOXB9*, *BMP4,* and endogenous controls *GAPDH* or *GUSB,* were amplified with pre-designed Taqman gene expression assay primers (Applied Biosystems). Expression data was acquired using an ABI Prism 7900HT Sequence Detection System (Applied Biosystems).

Sequencing and qPCR array for WNT pathway components: Genomic DNA was extracted from H2030, PC9, and their metastatic derivatives using the DNeasy kit (Qiagen). Sequencing was performed by the Geoffrey Beene Translational Oncology core facility. Putative exonic regions for the WNT pathway members: APC, APC2, AXIN1, AXIN2, CTNNB1, FRZB, GSK3B, LEF1, TCF7, TCF7L1, TCF7L2, SFRP1, SFRP2, SFRP4 and STK11 (NCBI Human Genome Build 36.1) were broken into "target regions" of 500 bp or less, and specific primers were designed using Primer 3. M13 tails were added to facilitate Sanger sequencing. PCR reactions were carried out in 384 well plates, in a Duncan DT-24 water bath thermal cycler, with 10 ng of genomic DNA as template, using a "touchdown" PCR protocol with HotStart Taq (Kapa Biosystems, Cape Town, South Africa). The touchdown PCR method consisted of: 1 cycle of 95°C for 5 min; 3 cycles of 95°C for 30 sec, 64°C for

30 sec, 72°C for 60 sec; 3 cycles of 95°C for 30 sec, 62°C for 30 sec, 72°C for 60 sec; 3 cycles of 95°C for 30 sec, 60°C for 30 sec, 72°C for 60 sec; 37 cycles of 95°C for 30 sec, 58°C for 30 sec, 72°C for 60 sec; 1 cycle of 70°C for 5 min. Amplified DNA was purified using AMPure (Agencourt Biosciences). The purified PCR reactions were split into two, and sequenced bidirectionally with M13 forward and reverse primer and Big Dye Terminator Kit v.3.1 (Applied Biosystems), at Agencourt Biosciences. Dye terminators were removed using the CleanSEQ kit (Agencourt Biosciences), and sequence reactions were run on ABI PRISM 3730xl sequencing apparatus (Applied Biosystems). Expression profiling for 84 WNT pathway-related genes was performed using the RT2 profiler qRT-PCR array system for WNT focused genes (SuperArray™).

Mutation detection. Mutation calls were produced using an automated detection pipeline at the MSKCC Bioinformatics Core. Bi-directional reads and mapping tables (to link read names to sample identifiers, gene names, read direction, and amplicon) were subjected to a QC filter which excludes reads that have an average phred score of < 10 for bases 100-200. Passing reads were assembled against the reference sequence (RefSeq) for each gene, containing all coding and UTR exons including 5Kb upstream and downstream of the gene, using command line Consed 16.0 (PMID: 9521923). Assemblies were passed on to Polyphred 6.02b (PMID: 9207020), which generated a list of candidate mutations, and to Polyscan 3.0 (PMID: 17416743), which generated a second list of putative mutations. The lists were merged together into a combined report, and the putative mutation calls were normalized to '+' genomic coordinates and annotated using the Genomic Mutation Consequence Calculator (PMID: 17599934). The resulting list of annotated mutations was loaded into a Postgres database along with select assembly details for each mutation call (assembly position, coverage, and methods supporting mutation call). To reduce the number of false positives generated by the mutation detection software packages, only mutations which are supported by at least one bi-directional read pair and at least one sample mutation called by Polyphred were considered, and only the putative mutations which are annotated as having non-synonymous coding effects, occur within 11 bp of an exon boundary, or have a conservation score > 0.699 (http://genome.ucsc.edu/cgi-bin/hgTrackUi?hgsid=108554407&g=multiz17way) were included in the final candidate list. Indels called by any method were manually reviewed and included in the candidate list if found to hit an exon.

Correlation coefficient analysis of Wnt3A responsive genes and clinical relapse. Parental and BrM3 derivatives from both cell models (H2030 and PC9) were mock treated or treated with Wnt3A. Duplicate samples were profiled for each condition, yielding 8 samples for each cell line model, for a total of 16 sample arrays. For the clinical samples, RMA was used as the pre-processing algorithm. We interrogated the prognostic value of a certain feature (e.g., the Wnt-response of H2030 parental cell line) with the following steps. First, the cognate cell line data (e.g., Wnt3a-treated H2030 vs. mock treated H2030, 4 chips altogether) were median-centered within chips (across all probes in the same chip) and then mean-centered across chips (for the same probe across the four chips). The same operations were performed on the clinical samples. Second, duplicated samples were averaged to yield a centroid vector for each sample under each condition. Third, a Pearson correlation coefficient was computed to gauge the similarity between each tumor sample and centroids from the cell line samples. The differences between correlation coefficients that are derived from the opposite centroids (e.g., Wnt3a-treated H2030 vs. mock treated H2030) were used to score the relative placement of this tumor between the two reference points. Lastly, we examined the association between the correlation coefficient scores and the clinical outcomes by fitting a Cox proportional hazards regression model (implemented by the "*coxph*" function of "*survival*" package in *R*). The correlation coefficients were computed using all available probes on the U133A_2 chips.

Derivation and validation of the Lung Cancer WNT Signature: Centroids derived from Wnt3A stimulation of H2030-BrM3 derivatives and parental PC9 cells yielded the most significant predictors of pathway activation and relapse. This is consistent with these derivatives being the most responsive to Wnt3A activation within each cell line model (see Results). The minimal list of

prognostic WNT-responsive genes was derived by first calculating a t statistic that represents the difference between the Wnt3a-treated vs. mock treated centroids using the following formula: $t = \frac{\overline{C1} - \overline{C2}}{S_{\overline{C1}\ \overline{C2}}}$, where $S_{\overline{C1}\ \overline{C2}} = \sqrt{\frac{s_1^2}{n_1} + \frac{s_2^2}{n_2}}$. $\overline{C1}$ and $\overline{C2}$ represent the mean expression values of the gene in the two centroids, respectively; s_1 and s_2 represent the standard deviations of the expression values among the replicate chips that comprise the two centroids; n_1 and n_2 are number of replicate chips underlying each centroid (in this case n=2). Next, we ranked all genes based on the t-statistics, removed genes whose t-statistics are lower than a certain threshold, calculated new correlation coefficient scores based on the truncated gene list, and evaluated the prognostic power of the new scores in MSKCC set I. We systematically increased the cut-offs of t-statistics to identify the shortest list of genes that still hold prognositic power in correlation coefficient analyses. In this manner 166 genes were identified for the H2030-BrM3 +/- Wnt3a centroids; and 109 genes identified for PC9-Parental +/- Wnt3a centroids. Both gene sets were verified to significantly correlate with increased metastatic potential. The fold changes of the 166 gene set under Wnt3a-treatment (compared to no treatment) significantly co-varied with their fold changes in Wnt3A stimulated H2030-BrM3 metastatic derivatives compared to their respective parental lines ($r=0.369$ $p<10^{-6}$). The 109 genes from PC9-Parental +Wnt3a centroid significantly co-varied with their fold changes in PC9-BrM3 metastatic derivatives compared to their respective parental lines under basal conditions ($r=0.645$, $p< 10^{-10}$). Because of limited overlap, the H2030-BrM3 and PC9 WNT responsive gene sets were combined to obtain a broader WNT classifier, filtering for genes that are statistically significantly altered between one set of centroids and display the same expression trend (by at least by15%) between the other set of centroids. 91 probes representing 81 unique genes remained to constitute the LWS-81. LWS-81 maintains the prognostic value in MSKCC set 1 and was independently confirmed in MSKCC set 2 by correlation coefficient analysis. Correlation coefficient scores for brain metastasis were calculated by specifically using the LWS. The performance of the LWS was unchanged across MSKCC set 1 and MSKCC set 2 when a more stringent 1.5 fold cutoff was applied in at least one centroid set.

To further gauge the performance of LWS-81, we clustered the two clinical datasets in an unsupervised manner (implemented by "*heatmap.2*" function of "*gplots*" package of *R*). To obtain the most robust clustering, we employed five different algorithms to define the distances between samples. These include Euclidean distance, absolute distance, Pearson's correlation coefficient, Spearman's correlation coefficient and Kendall's correlation coefficient. We then compared among the resulted clustering patterns using R-indices of clusters that are > 10% of the dataset (McShane et al., 2002). The algorithm that yielded the largest R-index was employed. This process was performed blind to clinical parameters and therefore is unbiased. We applied this clustering approach to MSKCC sets 1 and 2, as well as the SMC and 3 additional independent cohorts from (Shedden et al., 2008). In all cases, we could identify a cluster that expresses LWS-81 in the pattern more similar to that of Wnt3a-treated lung adenocarcinoma cell lines compared to the rest of the samples. Such clusters were defined as LWS+ and the rest of samples were defined as LWS-. The metastasis free survival of LWS+ and LWS- cohorts were then compared using log-rank test as implemented by *"survdiff"* function in the *"survival"* package of *R*.

To confirm our finding, we also performed a meta-gene analysis (Bild et al., 2006). In short, LWS genes were used to define a gene expression vector for each clinical sample or cell line (+Wnt3a vs. –Wnt3a). All vectors were then mean-centered (clinical samples and cell lines were processed separately) and were combined as a matrix. Next, we carried out principle component analyses on the combined matrix. The first principle components of clinical samples were compared to those of cell lines. Based on the relative positioning of the clinical samples between cell line models (+Wnt3a vs. –Wnt3a), a meta-gene score can be assigned to each sample. Such scores were then correlated with metastasis or survival. With these procedures, we were able to confirm the results from unsupervised clustering in MSKCC sets 1 and 2 ($p<0.001$ for both data sets).

LWS genes that were robustly up-regulated in both sets of BrM3 metastatic cells (Wnt3a treated and untreated) were selected as candidate metastasis mediators and functionally validated.

Supplemental References

Silva, J. M., Li, M. Z., Chang, K., Ge, W., Golding, M. C., Rickles, R. J., Siolas, D., Hu, G., Paddison, P. J., Schlabach, M. R.*, et al.* (2005). Second-generation shRNA libraries covering the mouse and human genomes. Nat Genet *37*, 1281-1288.

McShane, L. M., Radmacher, M. D., Freidlin, B., Yu, R., Li, M. C., and Simon, R. (2002). Methods for assessing reproducibility of clustering patterns observed in analyses of microarray data. Bioinformatics *18*, 1462-1469.

Bild, A. H., Yao, G., Chang, J. T., Wang, Q., Potti, A., Chasse, D., Joshi, M. B., Harpole, D., Lancaster, J. M., Berchuck, A.*, et al.* (2006). Oncogenic pathway signatures in human cancers as a guide to targeted therapies. Nature *439*, 353-357.

Table S1. Clinical annotation for two independent MSKCC primary lung adenocarcinoma cohorts used in this study. Percentages are provided in parentheses.

	MSKCC set 1	**MSKCC set 2**
Total	107	129
Mean Age (yrs)	64.7+/- 9.7	67.6+/- 11
Age range (yrs)	39-82	35-89
Male	45 (42)	50 (38.8)
Female	62 (58)	79 (61.2)
Stage		
IA	28 (26)	51 (39.5)
IB	37 (34.6)	37 (28.7)
IIA	4 (3.7)	4 (3.1)
IIB	19 (17.8)	8 (6.2)
IIIA	17 (15.9)	17 (13.1)
IIIB	2 (1.9)	7 (5.4)
IV	-	5 (3.9)
Recurrences	44 (41)	24 (18.6)

Table S2. List of 91 probe sets including 81 genes that constitute the lung cancer WNT responsive gene set (LWS). Expression based on MASS 5.0 normalized Affymetrix U133A_2 microarray data. In the third column, fold change of H2030-BrM3 cells stimulated with Wnt3A versus mock treated. The fourth column provides fold change for parental PC9 induced with Wnt3A.

Probe	Gene Symbol	H2030-BrM3 +Wnt3A	PC9+Wnt3A
204602_at	DKK1	3.70	1.93
211518_s_at	**BMP4**	**3.12**	**8.68**
216625_at	ROCK1	2.71	2.18
220943_s_at	C2orf56	2.71	1.19
209752_at	REG1A	2.54	4.92
209355_s_at	PPAP2B	2.33	1.51
204712_at	WIF1	2.32	1.23
221558_s_at	**LEF1**	**2.26**	**2.38**
205182_s_at	ZNF324	2.17	1.24
220410_s_at	CAMPSAP1	2.14	1.49
222224_at	NACA2	2.14	1.72
217204_at	MTRF1L	2.09	1.70
216417_x_at	**HOXB9**	**2.00**	**1.77**
202208_s_at	ARL4C	1.97	2.29
215594_at	PTR2 mRNA for repetitive sequence	1.97	1.90
202498_s_at	SLC2A3	1.80	1.72
208262_x_at	MEFV	1.74	1.18
204780_s_at	FAS	1.73	1.17
207944_at	LOC4951	1.73	1.33
219319_at	HIF3A	1.72	1.33
202207_at	ARL4C	1.71	2.38
209505_at	NR2F1	1.69	1.33
206355_at	GNAL	1.60	1.20
202497_x_at	SLC2A3	1.59	1.28
206391_at	RARRES1	1.57	1.45
210510_s_at	NRP1	1.51	1.22
202206_at	ARL4C	1.51	2.01
201739_at	SGK1	1.46	1.95
202499_s_at	SLC2A3	1.43	1.90
222088_s_at	SLC2A3	1.41	1.83
205214_at	STK17B	1.40	1.59
221283_at	RUNX2	1.40	2.87
201565_s_at	ID2	1.35	1.30
214579_at	NPAL3	1.34	3.03
216252_x_at	FAS	1.33	1.45
215719_x_at	FAS	1.32	1.22
218736_s_at	PALMD	1.31	2.04
204286_s_at	PMAIP1	1.29	1.61
201418_s_at	SOX4	1.21	1.35
207723_s_at	KLRC3	1.20	2.12
216909_at	RRP12	1.19	5.05
210585_s_at	TNPO2	1.19	2.10
202478_at	TRIB2	1.20	1.63

221544_s_at	MED16	1.17	1.17
205020_s_at	ARL4A	1.17	1.82
211647_x_at	IGHG1	1.16	1.16
207574_s_at	GADD45B	0.86	0.71
204368_at	SLCO2A1	0.86	0.72
207214_at	SPINK4	0.83	0.57
205778_at	KLK7	0.83	0.72
213247_at	SVEP1	0.81	0.22
213896_x_at	FAM149B1	0.81	0.87
201510_at	ELF3	0.81	0.81
210055_at	TSHR	0.80	0.69
220617_s_at	ZNF532	0.80	0.65
212173_at	AK2	0.80	0.61
204908_s_at	BCL3	0.79	0.85
206361_at	GPR44	0.78	0.75
219352_at	HERC6	0.77	0.85
216403_at	RP11-114G1.1	0.75	0.83
203910_at	ARHGAP29	0.75	0.86
212956_at	TBC1D9	0.75	0.82
207060_at	EN2	0.74	0.79
221009_s_at	ANGPTL4	0.73	0.64
216758_at	RAB33A	0.73	0.42
209101_at	CTGF	0.71	0.77
211380_s_at	PRKG1	0.70	0.46
205269_at	LCP2	0.67	0.19
209959_at	NR4A3	0.67	0.60
206803_at	PDYN	0.66	0.43
217555_at	SMC1A	0.65	0.48
216884_at	PTPN12	0.62	0.66
206646_at	GLI1	0.59	0.14
211368_s_at	CASP1	0.59	0.52
204758_s_at	TMEM24	0.58	0.45
36711_at	MAFF	0.58	0.78
215123_at	LOC23117	0.55	0.86
206715_at	TFEC	0.54	0.76
207560_at	SLC28A1	0.48	0.45
213715_s_at	KANK3	0.45	0.74
213638_at	PHACTR1	0.44	0.64
208134_x_at	PSG2	0.43	0.79
AFFX-LysX-5_at	NA	0.41	0.28
208552_at	GRIK4	0.35	0.46
208317_at	XYLB	0.35	0.49
216189_at	NA	0.34	0.49
215635_at	PDE8A	0.33	0.61
214998_at	AAK1	0.32	0.28
217022_s_at	IGHA1	0.31	0.81
204236_at	FLI1	0.29	0.25
209603_at	GATA3	0.23	0.80

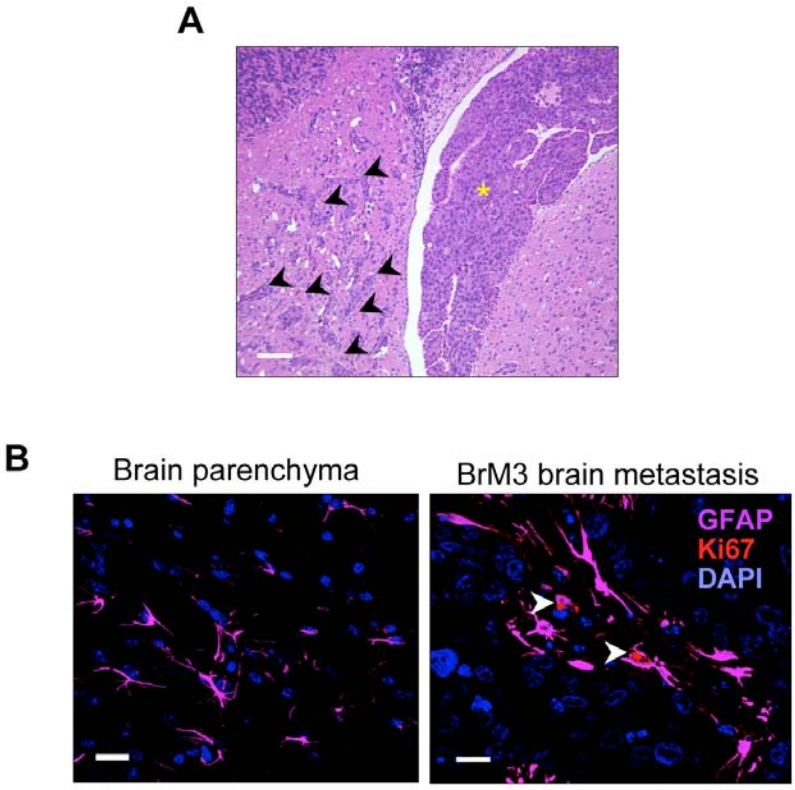

Figure S1.
(A) H&E staining of H2030-BrM3 brain metastasis. Arrows=small invasive lesions. *=leptomeningeal growth**.** Scale bars=100μm **(B)** Morphology and proliferation of astrocytes surrounding H2030-BrM3 lesions. Magenta=glial fibrillary acidic protein (GFAP). Arrows=murine Ki67 positive proliferating astrocytes (red). Scale bar=23μm.

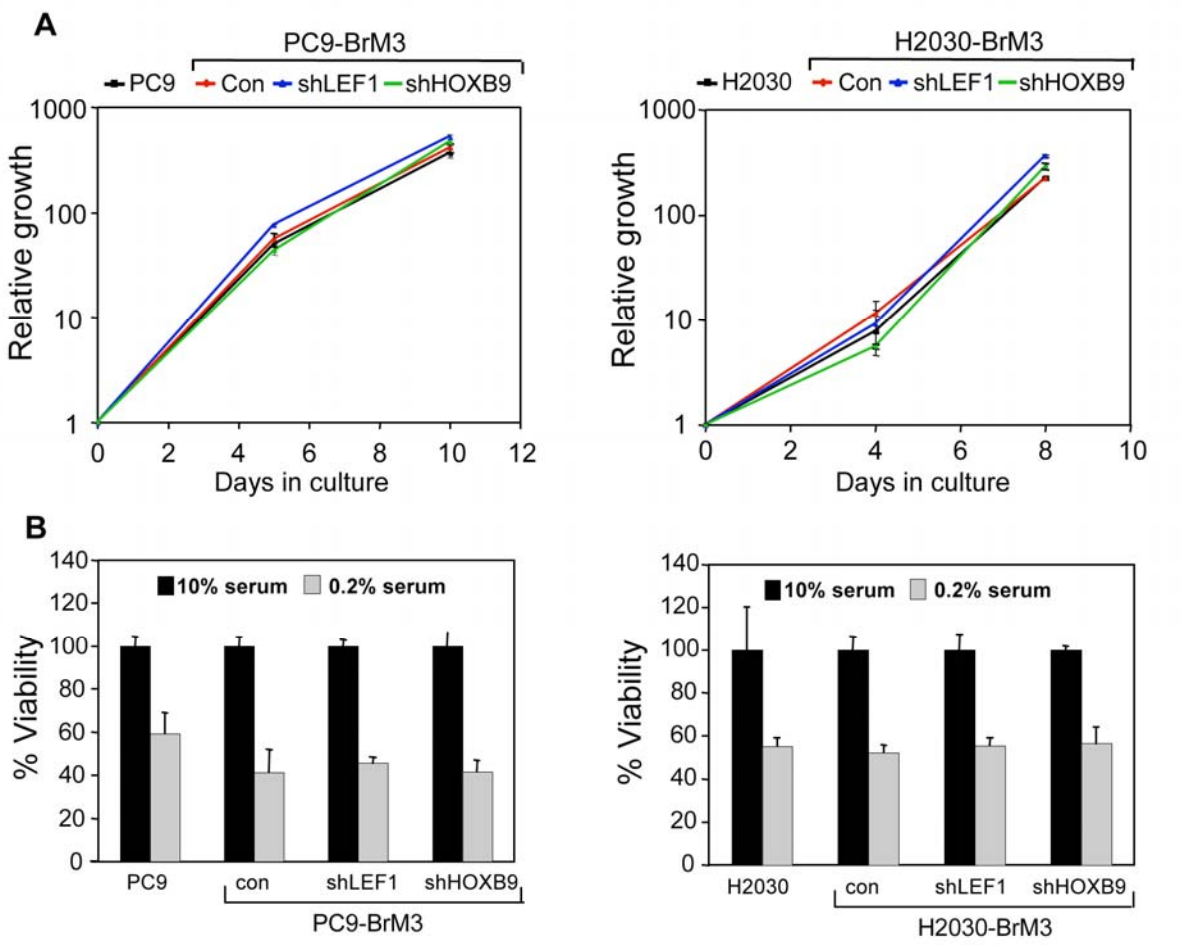

Figure S2. In vitro growth and viability.
(A) The growth kinetics of the indicated parental, BrM3 control, and BrM3 cells with *LEF1* or *HOXB9* knockdown were measured under monolayer conditions. **(B)** The indicated cell lines were deprived of growth factors and cell viability measured after five days. All error bars=SEM. p values based on a two-sided Student's t-test.

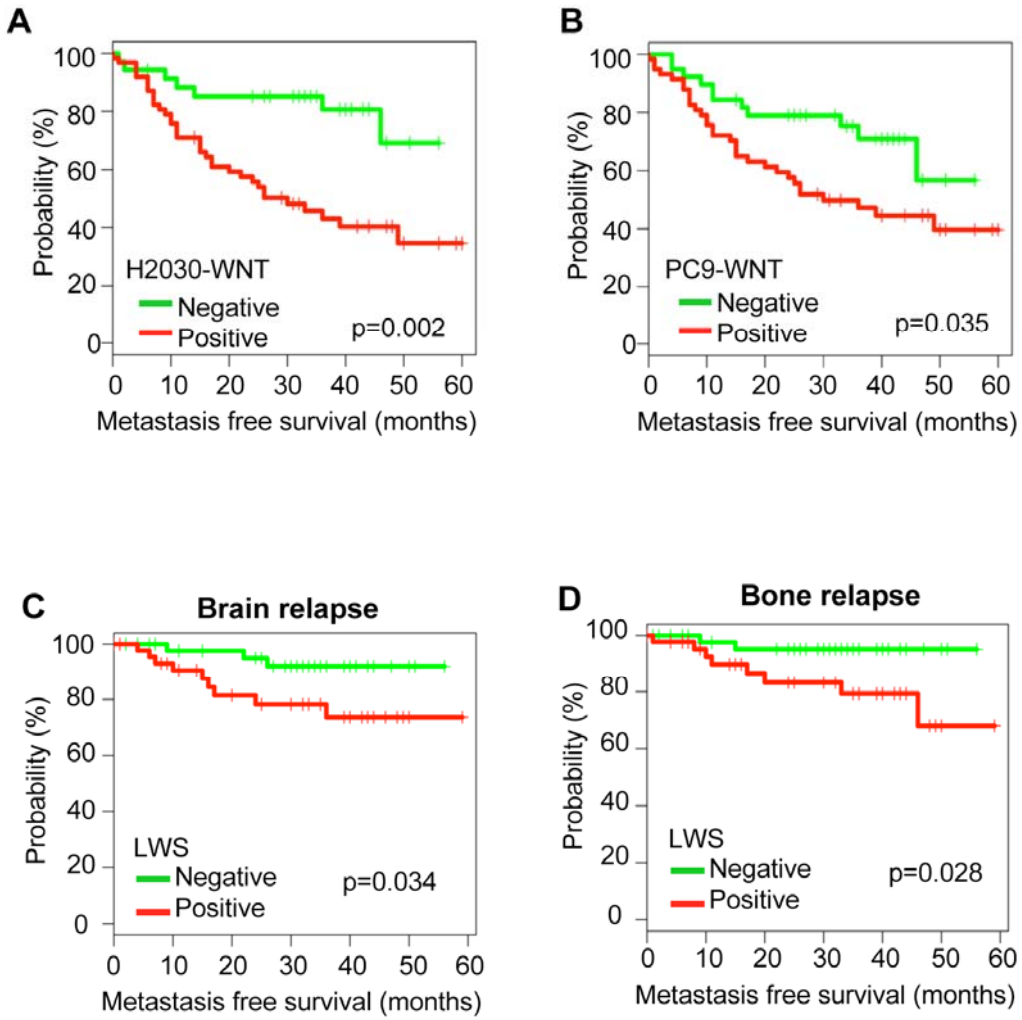

Figure S3. Derivation of the lung cancer WNT responsive gene set (LWS) and multi-organ recurrence.

H2030 and PC9 cells were mock treated or stimulated with Wnt3A for 3 hours. Correlation coefficient analysis for the combined WNT ligand gene response of parental and metastatic derivatives from each cell system (H2030 or PC9) was performed. **(A)** Kaplan-Meier curves for metastasis-free survival according to status of the H2030-WNT-responsive signature in the initial cohort of 107 primary lung adenocarcinomas (MSKCC set 1). Green=H2030-WNT negative; red=H2030-WNT positive. **(B)** Metastasis-free survival according to PC9-WNT-responsive signature in MSKCC set 1. The LWS is derived from a combination of Wnt3a regulated probe sets in the H2030-BrM3 derivatives and/or PC9-parental cells (See Supplemental Experimental Procedures). **(C)** Brain-specific metastasis according to LWS in primary tumors from MSKCC set 1. **(D)** Bone metastasis-free survival according to LWS in primary tumors from MSKCC set 1. p-values were calculated based on Log rank test.

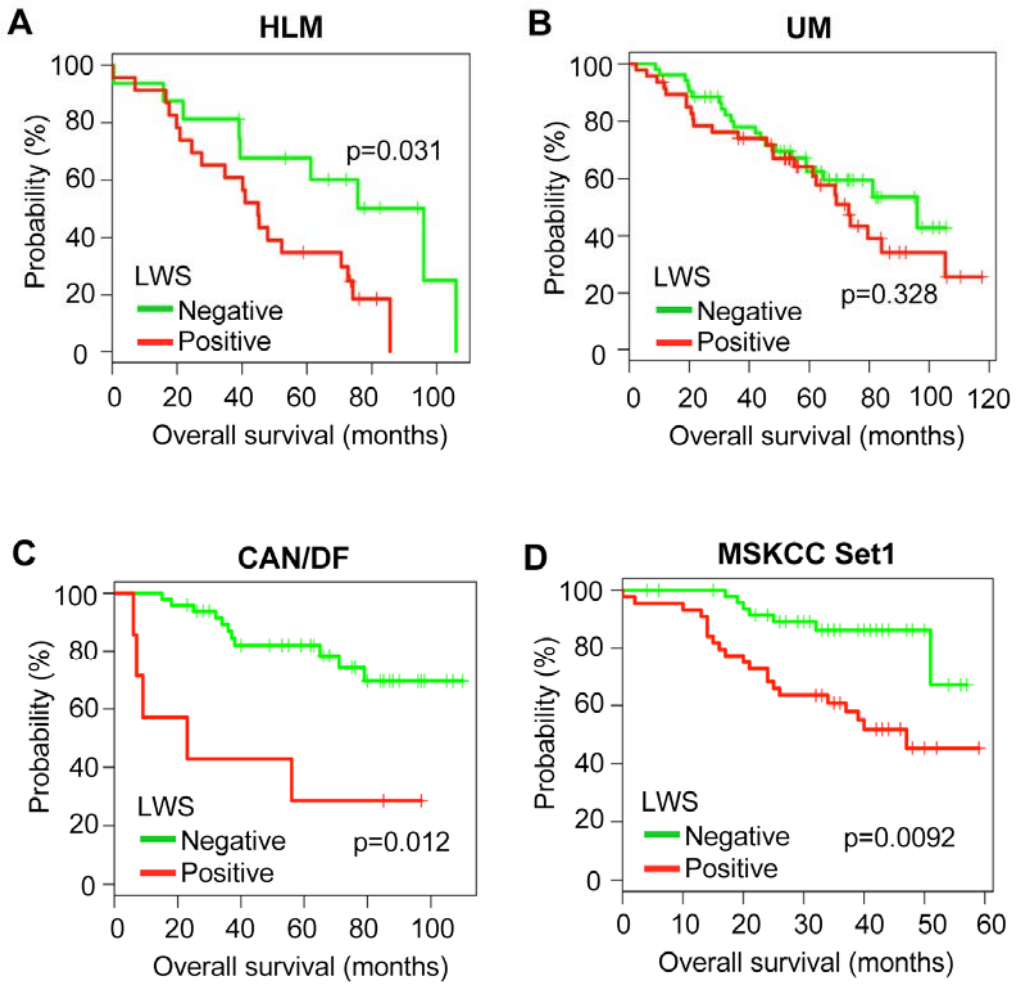

Figure S4. Overall survival based on LWS expression in stage I lung adenocarcinomas. Overall survival rates were determined based on LWS expression across four independent cohorts from (Shedden et al., 2008). These include stage I tumors from **(A)** the Dana Farber Cancer Institute (CAN/DF, n=56), **(B)** the University of Michigan Cancer Center (UM, n=116), **(C)** Moffit Cancer Center (HLM, N=41), and **(D)** samples from the Memorial Sloan-Kettering Institute that were included in MSKCC set 1 (total n=63). p-values were calculated based on Log rank test.

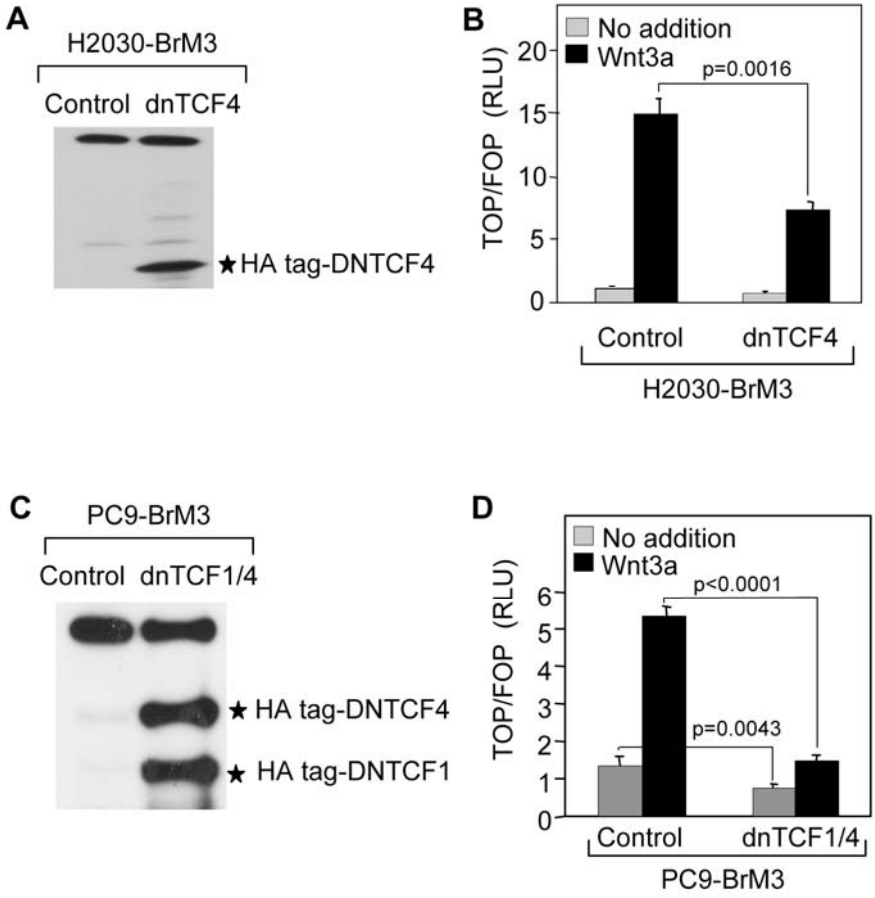

Figure S5. Stable dnTCF1/4 expression partially reduces LEF/TCF activity.
(A) H2030-BrM3 cells were infected with retrovirus encoding HA-tagged-dominant negative TCF4. Levels of dnTCF4 was assessed by immunoblot analysis of HA protein. **(B)** Control or dnTCF4 expressing cells were transfected with TOP/FOP-FLASH reporters, and LEF/TCF activity determined as in Figure 3B. **(C)** Both dnTCF1 and dnTCF4 were expressed in PC9-BrM3 cells and confirmed as in A. **(D)** LEF/TCF activity was measured as in B. Error bars=SEM.

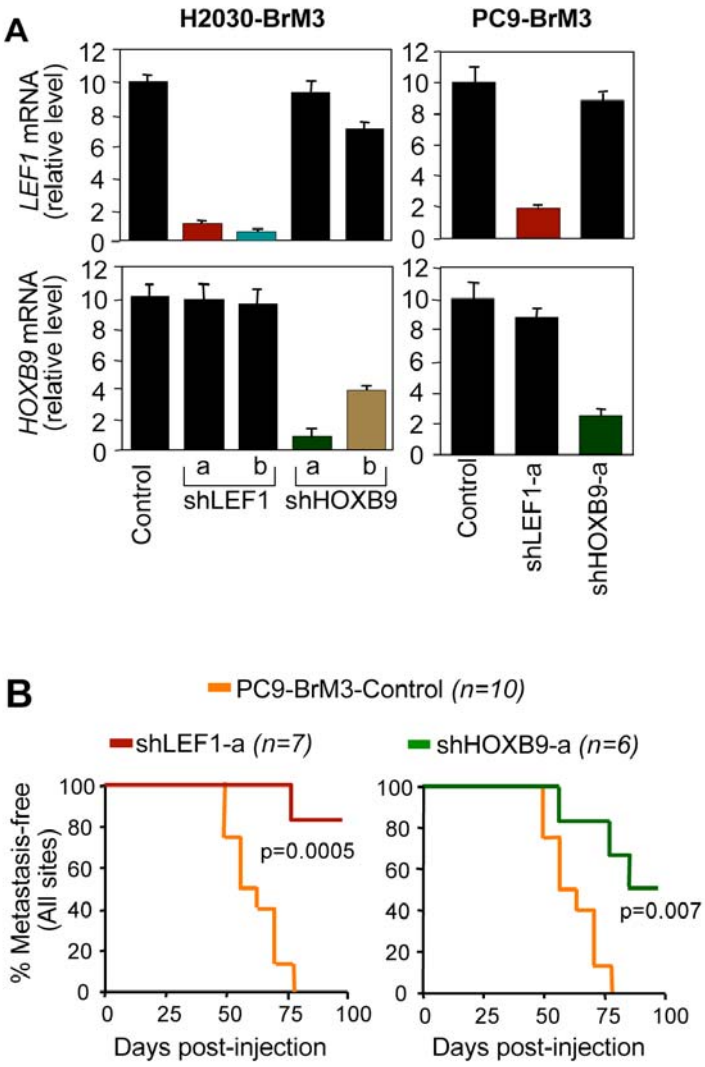

Figure S6. Knockdown of LEF1 and HOXB9.
(A) H2030-BrM3 cells were infected with retrovirus encoding independent hairpins (sh-a and sh-b) against *LEF1* or *HOXB9*. shLEF1-a and shHOXB9-a hairpins were stably expressed in PC9-BrM3 derivatives. Infected cells were selected and treated with Wnt3A for 3 hours before mRNA extraction. *LEF1* and *HOXB9* expression levels were confirmed by qRT-PCR. Error bars indicate 95% confidence interval for replicates. **(B)** Kaplan-Meier curves for overall metastasis-free survival of PC9-BrM3 control or PC9-BrM3 cells with the indicated gene knockdown was monitored following arterial inoculation. p-values were calculated based on Log rank test.

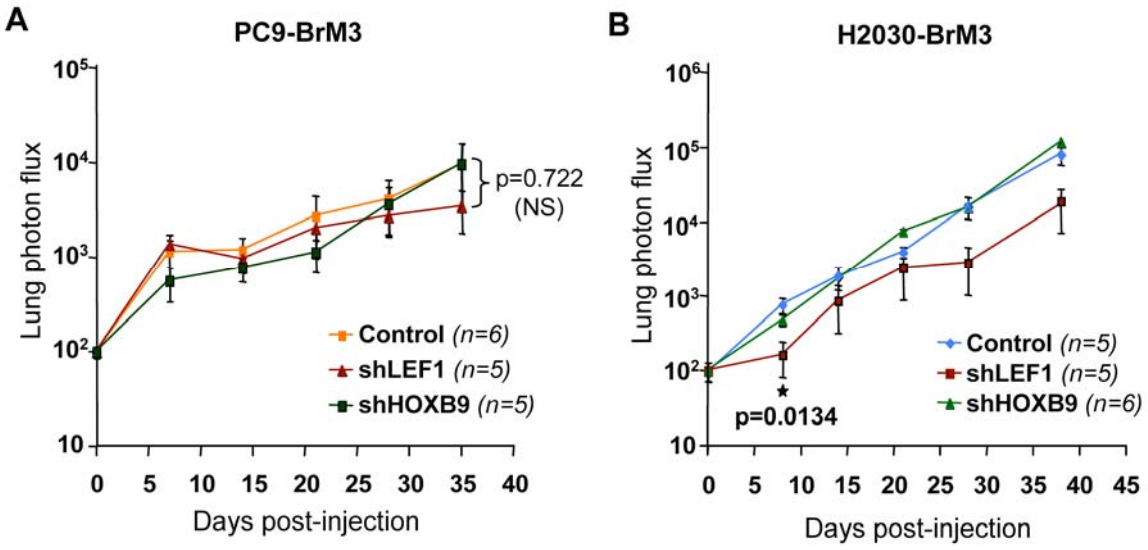

Figure S7. Effects of LEF1 and HOXB9 on lung tumorigenesis.
(A) PC9-BrM3 control or the indicated knockdown cells were implanted orthotopically with Matrigel. Lung tumor growth was measured as in Figure 2K. **(B)** The same experiment was performed with H2030-BrM3 control and the indicate lines. Error bars= SEM. p values based on a two-sided Student's t-test at the indicated time points.

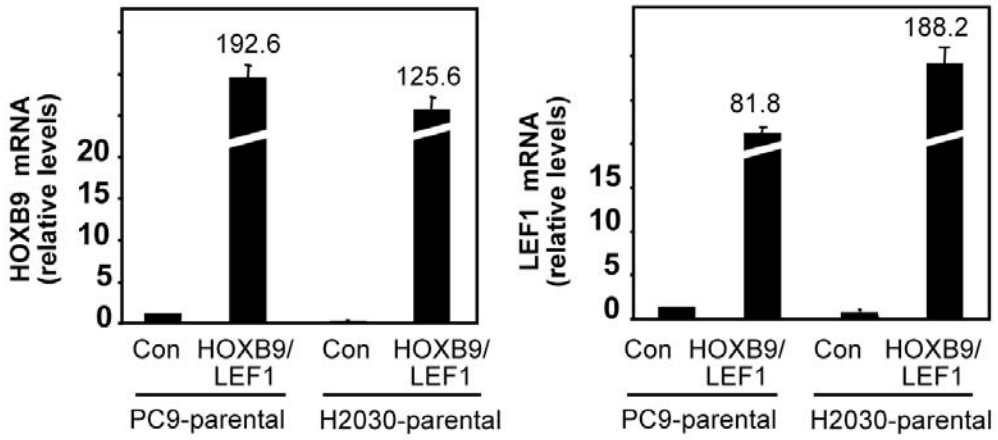

Figure S8. LEF1 and HOXB9 overexpression in parental PC9 and H2030 cells.
Retrovirus encoding LEF1 or empty vector control was used to infect PC9 or H2030 parental cells. Following puromicin selection, cells were super-infected with retrovirus encoding HOXB9 and the hygromicin resistance gene or empty vector control. Following hygromicin selection, expression of *LEF1* and *HOXB9* were measured by qRT-PCR. Error bars indicate 95% confidence interval for replicates**.**

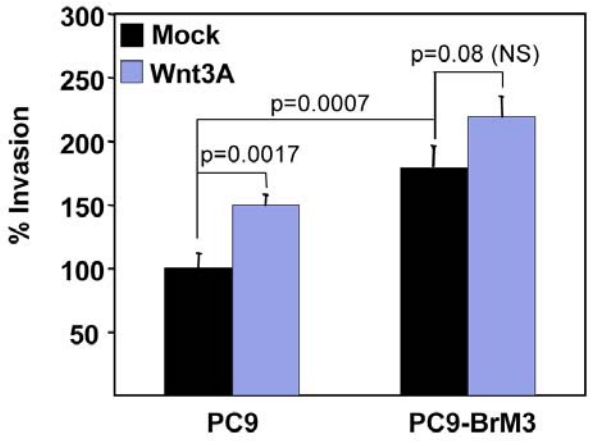

Figure S9. Invasion of PC9 parental and PC9-BrM3 cells.
Invasion assays were performed in the presence of astrocytes conditioned media in the bottom chamber. The indicated lines were used in the presence or absence of Wnt3A as in Figure 7. Error bars= SEM. p values based on a two-sided Student's t-test.

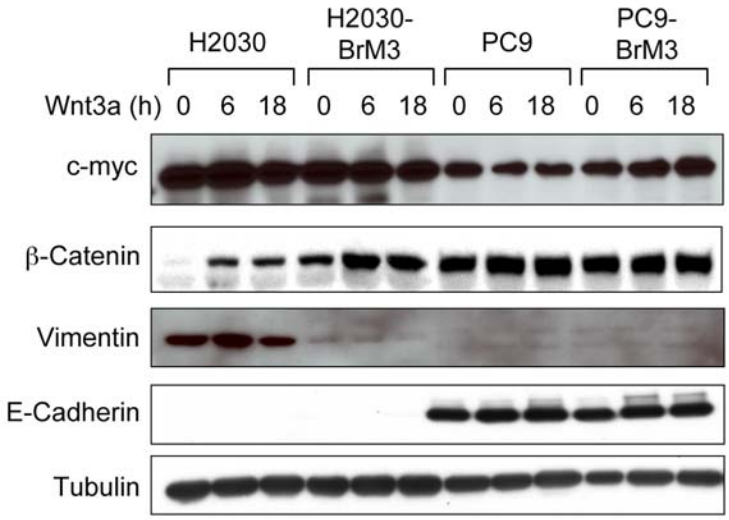

Figure S10. WNT response and metastatic potential do not correlate with c-myc or markers of EMT.
Immunoblot analysis for the indicated proteins extracted from cells treated with Wnt3A for 0, 6, and 18 hours.